Constraints on the pre-eruptive magma storage conditions and magma evolution of the 56–30 ka explosive volcanism of Ciomadul (East Carpathians, Romania)

Author(s):
Cserép, Barbara; Szemerédi, Máté; Harangi, Szabolcs; Erdmann, Saskia; Bachmann, Olivier; Dunkl, István; Seghedi, Ioan; Mészáros, Katalin; Kovacs, Zoltán; Virág, Attila; Ntaflos, Theodoros; Schiller, David; Molnár, Kata; Lukács, Réka

Publication date:
2023-12

Permanent link:
https://doi.org/10.3929/ethz-b-000646219

Originally published in:
Contributions to Mineralogy and Petrology 178(12), https://doi.org/10.1007/s00410-023-02075-z

Funding acknowledgement:
214930 - Dynamics of magma reservoirs in polybaric differentiation columns in the earth's crust; an integrated approach (SNF)

Contributions to Mineralogy and Petrology (2023) 178:96
https://doi.org/10.1007/s00410-023-02075-z

ORIGINAL PAPER

Constraints on the pre-eruptive magma storage conditions and magma evolution of the 56–30 ka explosive volcanism of Ciomadul (East Carpathians, Romania)

Barbara Cserép[1,2] · Máté Szemerédi[1,3] · Szabolcs Harangi[1,2] · Saskia Erdmann[4] · Olivier Bachmann[5] · István Dunkl[6] · Ioan Seghedi[7] · Katalin Mészáros[2] · Zoltán Kovács[1,8] · Attila Virág[2,9] · Theodoros Ntaflos[10] · David Schiller[11] · Kata Molnár[12] · Réka Lukács[1,13]

Received: 4 January 2023 / Accepted: 27 October 2023 / Published online: 28 November 2023

Abstract

A detailed mineral-scale study was conducted on pumices of the latest, dominantly explosive eruption epoch (56–30 ka) of Ciomadul, the youngest, long-dormant volcano in eastern-central Europe for characterizing the magma storage system and for understanding better the changes in eruption style from effusive to explosive. The mineral cargo of dacitic pumices enables us to constrain the conditions of the pre-recharge crystal mush, the recharge magmas and the post-recharge magma prior to eruptions. A careful evaluation of the results yielded by various thermometers, barometers, oxybarometers, chemometers and hygrometers as well as direct comparison with experimental data were necessary to select the appropriate techniques and therefore to constrain the conditions for the Ciomadul magmatic system. Beneath the volcano, a felsic crystal mush body is inferred at 8–12 km depth comprising slightly oxidized (0.5–1.6 ΔNNO), low-temperature (680–750 °C), highly crystalline magma. This zone is underlain by a deep magma storage zone with less evolved, hot (> 900 °C) magma at 16–40 km depth. The dominantly explosive volcanism after the effusive eruptions (160–90 ka) can be explained by the ascent of distinct recharge magmas. They contained high-Mg (MgO > 18 wt%) amphibole, which could have crystallized from ultrahydrous (H_2O > 8 wt%) magma at near-liquidus conditions. The rates of amphibole overgrowth and microphenocryst formation require weeks to months for the magma mixing and the eruption events. The hybridized melt became more oxidized and contained dissolved water in around 5.5 wt% at temperature of 790–830 °C calculated from the re-equilibrated Fe-Ti oxides. These magma properties along with the degree of crystallinity (27–38 vol% crystals) favored rapid magma ascent and an explosive style eruption. Thus, the strongly hydrous nature of the recharge magma in addition to the crystallinity and H_2O content of the pre-eruption magma plays an important role in controlling the eruption style.

Keywords Geothermobarometry · Oxybarometry · Pre-eruptive conditions · Eruption style · Recharge magma · Magma reservoir · Ciomadul

Introduction

Eruption of volcanoes—irrespective of their magnitude—poses a significant, but often underrated risk on modern society. This requires an improvement of knowledge of when, why and how volcanoes erupt and how such events can be forecasted (e.g., Sparks 2003; Cashman and Sparks 2013; Newhall et al. 2018; Papale and Marzocchi 2019; Poland and Anderson 2020; Mani et al. 2021; Cassidy and Mani 2022). The potential for an eruption, as well as the style of the volcanic activity, i.e., effusive or explosive, primarily depend on the physicochemical state of the subvolcanic magma storage system, the eruption trigger mechanism and its timescale (Cassidy et al. 2018; Costa et al. 2020; Popa et al. 2021a, b; Chakraborty and Dohmen 2022; Giordano and Caricchi 2022; Mangler et al. 2022). They can be inferred from the volcanic products of past eruptions, therefore petrology plays a crucial role in eruption forecasting and mitigation

Communicated by Timothy L. Grove.

Barbara Cserép and Máté Szemerédi have contributed equally to this work.

Extended author information available on the last page of the article

(Saunders et al. 2012; Gansecki et al. 2019; Nurfiani et al. 2021; Bindeman et al. 2022; Pankhurst et al. 2022).

Most volcanoes are underlain by complex trans-crustal magma storage systems with two major parts (Annen et al. 2006; Bachmann and Huber 2016): (1) a lower crustal hot zone, where mafic magmas are accumulated and evolve to lower density intermediate magma, which can intrude into the upper crust to build (2) an upper crustal felsic magma reservoir, which consists mostly of physically un-eruptible highly crystalline mush formed by repetitive magma recharge from which occasionally eruptible magma batches develop. While the felsic magma reservoirs can have a prolonged lifetime of several 10's to 100's thousand years, rejuvenation leading to eruption is a fast process lasting only weeks to years (e.g., Morgan et al. 2006; Burgisser and Bergantz 2011; Druitt et al. 2012; Matthews et al. 2012; Cooper and Kent 2014; Cooper 2019; Sundermeyer et al. 2019; Conway et al. 2020). This holds also for long-dormant volcanoes, which are in an apparent quiescent state for hundreds to even several tens of thousands years before rapid reawakening (e.g., Chaitén, Chile, Pinatubo, Philippines; Castro and Dingwell 2009; Burgisser and Bergantz 2011). Long volcano dormancy decreases awareness, although existence of a melt-bearing subvolcanic magma reservoir enables potential reactivation of an otherwise un-eruptible mushy magma body (crystal mush). For such seemingly inactive volcanic systems showing no signs of unrest for over ten thousand years but with indication for melt-bearing magma storage beneath, Harangi et al. (2015a, b) suggested the term PAMS volcano, i.e., a volcano with potentially active magma storage.

To predict whether a highly crystalline magma body beneath a PAMS volcano is capable of rejuvenation and if so, what kind of eruption can be expected, remains a challenging task with an impact to local and global society. Constraining pre-eruptive magma storage conditions of past eruptions, particularly those following long dormancy, can help to understand better the behavior of such volcanic systems and to identify early warning signs for reactivation. Pre-eruption physicochemical parameters, such as magma temperature (T), pressure (P), redox state (fO_2), water (H_2O) concentration as well as crystallinity strongly influence the trigger and style of eruptions (e.g., Nagasaki et al. 2017; Cassidy et al. 2018; Popa et al. 2019, 2021a, b). To constrain these parameters for pre-eruptive and long-term storage conditions, results of phase equilibrium experiments can be directly used or several mineral ± melt chemometers, thermometers, barometers and oxybarometers can be employed. Accessory minerals, such as zircon and titanite are typically low-temperature (< 800 °C) phases, which are stable in the crystal mush for prolonged periods, whereas Fe-Ti oxides re-equilibrate rapidly in a matter of days (Venezky and Rutherford 1999; Morgado et al. 2019; Prissel et al. 2020; Hou et al. 2021) and therefore reflect closely the post-rejuvenation magma condition. Other phases, such as Ca-amphiboles, pyroxenes, and plagioclase can be used to constrain both magma storage states that of the long-lived mush storage and that immediately prior to eruption. A vast number of chemometer, thermometer, barometer and oxybarometer calibrations exists, which have been defined for different conditions, compositional systems or phase assemblages and at highly variable accuracy. Careful selection is required to employ appropriate methods that derive robust and accurate estimates for a particular magmatic system.

In this study, we constrain the pre-eruptive and long-term magma storage conditions for the youngest (56–30 ka), dominantly explosive eruption period of Ciomadul volcano (Carpathian–Pannonian Region, Romania; Szakács et al. 1993, 2015; Harangi et al. 2015a, b, 2020; Karátson et al. 2019; Lahitte et al. 2019; Laumonier et al. 2019; Molnár et al. 2019; Lukács et al. 2021). Combined geophysical, petrological, and thermal modelling results indicate that a melt-bearing magma body can still exist in the upper crust beneath the volcano (Szakács et al. 2002; Popa et al. 2012; Harangi et al. 2015b; Laumonier et al. 2019; Lukács et al. 2021). Therefore, rejuvenation of the volcanic activity remains a possibility and volcanic hazard cannot be ignored (Szakács and Seghedi 2013) in spite of the long, 30 ka dormancy of the volcano. Zircon-based eruption chronology studies (Molnár et al. 2018, 2019) have pointed out that during the lifetime of Ciomadul volcano, reawakening after several 10's and even > 100 ka long quiescence period occurred several times. The mineral assemblage of the Ciomadul high-K dacite is suitable to evaluate critically the pre-eruption conditions of the volcano, providing new constraints for hazard assessment and monitoring.

Geological background

Ciomadul (Fig. 1) is located in eastern-central Europe, in the eastern part of the Carpathian–Pannonian Region, which has experienced volcanic activity for the last 20 Ma in response to the formation of the Pannonian Basin with lithospheric thinning as well as subduction and collision along the Carpathians (Szabó et al. 1992; Seghedi et al. 1998; 2004, 2019; Harangi 2001; Konečný et al. 2002; Harangi and Lenkey 2007; Seghedi and Downes 2011). Ciomadul is associated with a post-collisional setting, where most of the volcanic eruptions occurred well after the collision of the Tisza-Dacia block with the East European Platform at around 11 Ma (Mațenco and Bertotti 2000) along a former retreating subduction boundary (Royden et al. 1982). The volcanic complex developed on a fold-and-thrust belt of Cretaceous flysch nappes, which form an arcuate belt along the outer foreland of the Carpathian orogen (Roure et al. 1993). The volcano

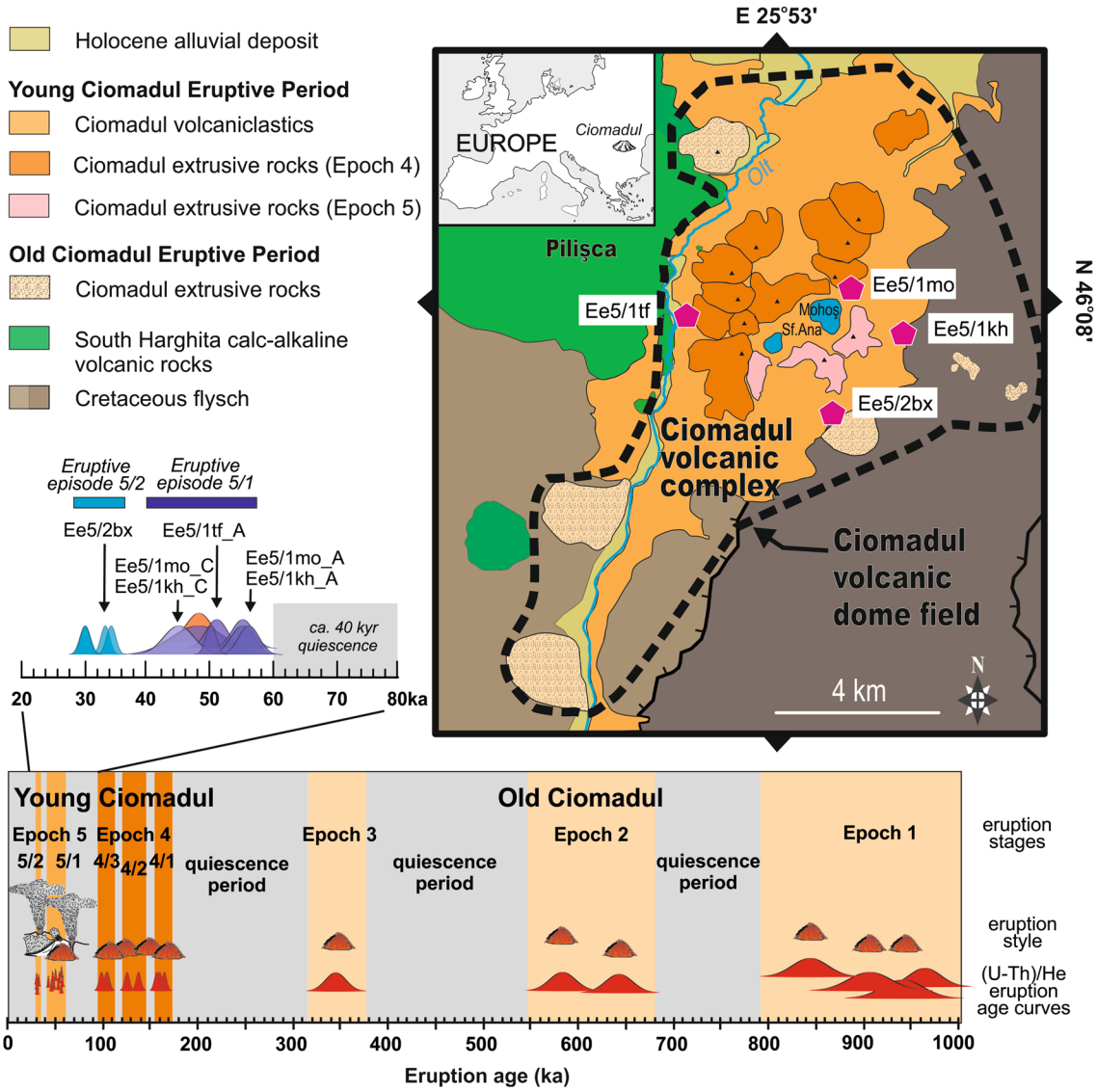

Fig. 1 Geological map and eruption history of the Ciomadul volcanic complex, Eastern Carpathians (Romania), showing our sampling localities (Ee5/1tf, Ee5/1mo, Ee5/1kh, Ee5/2bx). Modified after Lukács et al. (2021) and based on Seghedi et al. (1987). Sample details are summarized in Table 1

is located in a geodynamically still active area, close (ca. 70 km) to the Vrancea zone, one of the most active seismic zones in Europe, where a near-vertical descending slab causes frequent earthquakes with deep hypocentres (Wenzel et al. 1998).

Ciomadul is the southernmost eruptive system of the Călimani–Gurghiu–Harghita andesitic-dacitic volcanic chain, which extends over 160 km in NW–SE direction along the Eastern Carpathians (Romania; Mason et al. 1995, 1996; Szakács et al. 2015). It represents the latest manifestation of the volcanism, which shows gradual younging towards the southeast from 11 to 0.03 Ma (Pécskay et al. 2006). In addition, Ciomadul generated the youngest eruptions in the entire Carpathian–Pannonian Region and in eastern-central Europe, where the latest eruption occurred at ~ 30 ka (Harangi et al. 2010, 2015b, 2020; Lahitte et al. 2019). Ciomadul comprises a volcanic dome field with a massive volcanic complex in its centre (Szakács et al. 2015; Karátson et al. 2016, 2019; Molnár et al. 2018, 2019). The peripheral dacitic, andesitic, and shoshonitic lava domes formed episodically between 1 Ma and 300 ka, during the Old Ciomadul Eruptive Period (OCEP; Molnár et al. 2018). The central volcanic complex is composed mostly by amalgamated lava domes with a volume of ca. 10 km^3 (Szakács et al. 2015; Karátson et al. 2019) and is developed within the last 160 ka during the Young Ciomadul Eruptive Period (YCEP; Molnár et al. 2019). During the evolution of Ciomadul, long (several

10's of ka) quiescent periods occurred (Molnár et al. 2019), that were usually longer than the elapsed time since the youngest eruption (~ 30 ka) of the volcanic complex. Eruptions of the YCEP occurred in two epochs (Molnár et al. 2019). From 160 to 90 ka, several dacitic lava extrusions formed a southwest-northeast trending, elongated dome complex. From 56 to 30 ka, after a prolonged quiescence period, volcanic activity recommenced with mostly explosive eruptions (Vulcanian to sub-Plinian), which formed two deep craters, now filled by the Mohoş peat bog and the St. Ana crater lake (Szakács and Seghedi 1989; Vinkler et al. 2007; Karátson et al. 2016, 2019; Szakács et al. 2015; Harangi et al. 2020).

Several lines of evidence suggest a potentially active magma storage beneath Ciomadul (Popa et al. 2012; Harangi et al. 2015a, b; Laumonier et al. 2019; Lukács et al. 2021), thus classifying it as a characteristic "PAMS" volcano. First, zircon dates are consistent with prolonged (several 100's of thousand year long) existence of crystal mush storage and repeated rejuvenations (Harangi et al. 2015a; Lukács et al. 2021). Second, geophysical anomalies (i.e., low electrical resistivity and seismic wave attenuation) suggest the existence of a melt-bearing subvolcanic plumbing system with calculated average melt fractions of ~ 5–15 vol% (Popa et al. 2012; Harangi et al. 2015b), but locally perhaps up to ~ 40–50 vol% (Laumonier et al. 2019). The active character of the volcanic center is moreover underscored by significant, ongoing diffuse CO_2-emanations, which comprise a strong magmatic component (Kis et al. 2017, 2019). Eruptions of Ciomadul are fed by compositionally homogeneous, high-K dacitic magmas (Molnár et al. 2018, 2019) with notably high Sr/Y (Fig. 1; Szakács et al. 1993; Seghedi et al. 1987, 2023; Molnár et al. 2018, 2019). The magmas are crystal-rich (25–40 vol%), containing plagioclase, calcic amphibole, and biotite phenocrysts and zircon, apatite, titanite, and Fe-Ti oxides as accessories (Vinkler et al. 2007; Kiss et al. 2014). High-Mg minerals (clinopyroxene, orthopyroxene, olivine) occur often in various amounts either within amphibole phenocrysts or as crystal clots. Felsic crystal clots of plagioclase, amphibole, biotite, accessory phases, and intercrystalline glass are ubiquitous. Quartz and K-feldspar are found occasionally in some of the older (130–100 ka) lava dome rocks (Kiss et al. 2014). Amphibole is ubiquitous in the dacites and shows complex zoning patterns and chemical variability (Kiss et al. 2014; Harangi et al. 2015a; Laumonier et al. 2019), resembling amphibole populations reported for Mt. Pinatubo (Pallister et al. 1996), Soufriére Hills (Murphy et al. 2000), Mt Pelée (Pichavant et al. 2002), Unzen (Sato et al. 2005), Mt St. Helens (Thornber et al. 2008) and Redoubt (Coombs et al. 2013) volcanoes, among others.

Samples

Within the latest eruptive period of Ciomadul (Eruptive Epoch 5; Ee5, Molnár et al. 2019), two eruptive episodes—denoted as Ee5/1 (56–44 ka) and Ee5/2 (34–30 ka)—were distinguished based on combined (U-Th)/He and U-Th ages (Harangi et al. 2015a, 2020; Molnár et al. 2019). The volcanic products are mostly pumiceous pyroclastic deposits formed by Vulcanian and sub-Plinian eruptions and ash beds of phreatomagmatic events with a single identified lava dome of the 48 ka Piscul Pietros (Szakács and Seghedi 1989; Vinkler et al. 2007; Szakács et al. 2015; Karátson et al. 2016, 2019; Molnár et al. 2019; Harangi et al. 2020). The abundance of cracked, glassy volcanic blocks found in ravines and in pyroclastic flow deposits nevertheless implies multiple lava dome extrusions, which were destroyed entirely by subsequent explosive eruptions. Exposures are limited in the strongly vegetated area, but pyroclastic beds are locally well-exposed (Fig. 1, Fig. S1). In this study, we focus on the Vulcanian to sub-Plinian pumiceous explosive eruption products. Based on a thorough petrological and geochemical characterization, ten samples from three eruption units were selected for a more detailed study. Sample localities and outcrop details are shown in Fig. 1 and Figure S1 (in Electronic Supplementary Material 1; ESM 1), respectively.

Six of our samples are from Eruptive episode 5/1 (Ee5/1) and four samples are from Eruptive episode 5/2 (Ee5/2). An up to 3 m thick, medium to well-sorted pyroclastic unit composed of pumice lapilli around the Mohoş crater (Fig. 1) represents the first explosive eruption event, which was discharged after a long (35–40 ka) quiescence period of Ciomadul. The lapilli bed is exposed at the lower part of the Covasna-Harghita frontier outcrop (unit Ee5/1kh_A; same locality as MK-4 of Harangi et al. 2015a, Bolondos outcrop, BOL-1 of Karátson et al. 2016, and KH of Molnár et al. 2019) and in the recently excavated Mohoş roadcut (unit Ee5/1mo_A; same locality as Mohoş, Vârful Mohoş, MOH-VM of Karátson et al. 2016 and locality-226 of Molnár et al. 2019). Zircon from both localities shows the same (U-Th)/He age of 56 ± 4 ka (Molnár et al. 2019), and we therefore group them as the Ee5/1–56 eruption unit. Pumices from the upper part of a series of lapilli beds (unit Ee5/1tf_A), occurring beneath massive pyroclastic flow and phreatomagmatic units exposed in the abandoned Băile Tuşnad quarry (Vinkler et al. 2007; Szakács et al. 2015) at the western segment of the volcano (Fig. 1), represent a 50.3 ± 1.3 ka explosive eruption event (Harangi et al. 2015a). This locality is denoted as Tuşnad by Vinkler et al. (2007), MK-3 by Harangi et al. (2015a), and BTS-1 by Karátson et al. (2016). We refer to this unit as Ee5/1–50.

The youngest, 5/2 eruptive episode consists of Vulcanian and sub-Plinian pumiceous deposits and

phreatomagmatic beds occurring in ravines and as distal tephra beds around the volcano (Vinkler et al. 2007; Harangi et al. 2015a, 2020; Karátson et al. 2016; Molnár et al. 2019). For this study, we selected pumice samples from the most extensively studied block-and-ash flow deposit (Vinkler et al. 2007; Harangi et al. 2010, 2015a), exposed at the Bixad-Balvanyos roadcut at the southern slope of the volcano (unit Ee5/2bx). This outcrop was sampled as locality MK-5 by Harangi et al. (2015a) and as BIX-1 by Karátson et al. (2016). The eruption age is constrained by radiocarbon dates on charcoal fragments and zircon (U-Th)/He dates giving an age of 31.05–31.94 ka cal BP and 32.6 ± 1.0 ka, respectively (Harangi et al. 2010; 2015a), thus we refer to the unit as Ee5/2–32.

The studied samples are dacitic pumices and their main features are summarized in Table 1. The pumice lapilli and blocks contain euhedral to anhedral macrocrysts (> 500 µm size) and mesocrysts (100–500 µm size; cf. terminology proposed by Zellmer 2021), felsic ± mafic crystal clots in a glassy, microlite-bearing (~ 1–14 vol%), strongly vesiculated matrix. Vesicles are irregular to elongate. The microcrysts (1–100 µm size) and macrocrysts make up 8–19 vol%, comprising plagioclase and amphibole, as well as minor amounts of biotite (Table 1). Felsic crystal clots (~ 0.5–2 vol%), comprising plagioclase, amphibole, biotite, and accessory apatite, titanite, zircon, and Fe-Ti oxides, occur in various amounts. Mafic crystal clots (0.1–3 vol%) of orthopyroxene and/or clinopyroxene overgrown by amphibole, occur exclusively in pumice of unit Ee5/1–56.

Methods and used data

Petrological characterization of the studied samples was performed by combined application of optical and scanning electron microscopy at the Department of Petrology and Geochemistry, Eötvös Loránd University, Budapest, Hungary. Back-scattered electron (BSE) images were produced by an AMRAY 1830 I/T6 scanning electron microscope using the following conditions: 20 kV accelerating voltage, 1 nA beam current, and 1 s acquisition time. Crystal content (vol%; crystallinity; Popa et al. 2020) was estimated by point counting of macrocrysts using optical and back-scattered electron images from representative thin sections of each eruption unit. We used the JMicroVision v1.3.4 software for this purpose (Roduit 2022). Minor to accessory Fe-Ti oxides, zircon, and titanite are important for our study, therefore they were recovered from mineral separates prepared following standard heavy mineral separation methods (see details in Harangi et al. 2015a; Molnár et al. 2019). Crystals were fixed on double-sided adhesive tape and then embedded in 25 mm diameter epoxy mounts. Crystal mounts were

Table 1 Key information for the selected samples of the three eruption units

Eruption unit	Locality/localities	GPS coordinates	Eruption age (ka)	Crystallinity (on vesicle-free basis, avg. vol%)	Vesicles (avg. vol%	Groundmass (glass + microlites avg. vol%)	All crystals (avg. vol%)	Plg (avg. vol%)	Am (avg. vol%)	Bt (avg. vol%)
Ee5/2–32	Bixad	N46°5′59.65″ E25°52′53.85″	32.6 ± 1.0	38	49	21 + 11	19	11	6	2
Ee5/1–50	Băile Tuşnad	N46°7′54.89″ E25°51′35.09″	50.3 ± 1.3	29	71	20 + 1	9	7	1	< 1
Ee5/1–56	Covasna-Harghita border, Mohoş roadcut	N46°7′46″ E25°55′54″ N46°8′13.74 E25°54′34.03″	55.9 ± 2.0 55.0 ± 5.0	27	63	19 + 8	10	5	4	1

Eruption ages are combined U-Th(-Pb) and (U-Th)/He ages (Harangi et al. 2015a; Molnár et al. 2019). Relative volume (vol%) is modal estimation based on point counting of representative thin sections for each eruption unit. Crystallinity is given as vesicle-free meso- and macrocryst content (vol%)

lapped by 2500 mesh SiC paper and polished by diamond suspensions.

Chemical composition of minerals and glasses selected by the preliminary petrologic study was quantitatively determined by electron probe microanalysis (EPMA) using WDS detectors. Most of the analyses were conducted using a JEOL JXA 8900 RL electron microprobe at the Geozentrum, Georg-August University, Göttingen, Germany. Analyses of amphibole, plagioclase, glass, and Fe-Ti oxides were performed at 15 kV and 15 nA, using a defocused beam with a diameter ranging from 2 to10 µm. For glass measurements, the NMNH111240-52, VG-2 Smithsonian Microbeam Standard were used with 0.02 wt% H_2O content. During the glass session, F and Cl were also measured. This data set was complemented by analytical results obtained using a CAMECA SX100 electron microprobe at the Department of Lithospheric Research, University of Vienna, Austria. Analyses of amphibole, plagioclase, and glass was performed at 15 kV and 20 nA, using a defocused beam of 3–5 µm, respectively. Additional analyses were performed with a Cameca SX Five electron microprobe at the Institut des Sciences de la Terre d'Orléans—Centre National de la Recherche Scientifique (ISTO-CNRS), Orléans, France. Analyses of plagioclase, amphibole, orthopyroxene, and clinopyroxene were performed at 15 kV and 15 nA, using a defocused beam of ~ 10 µm. Repeating analyses on selected crystals were used to ascertain inter-laboratory correlation. Synthetic and natural minerals and synthetic glasses were used as standards. Amphibole Fe^{3+} value was estimated based on the IMA recommendation (Leake et al. 1997; Schumacher 1997) what is consistent with the method suggested by Holland and Blundy (1994). In the text, we report glass data normalized to 100% on an anhydrous basis.

Trace element compositions of accessory minerals (zircon and titanite) were determined by laser ablation inductively coupled mass spectrometry (LA-ICP-MS). Zircon trace element compositions are those already published by Lukács et al. (2021), which were measured at the Geochronology laboratory, ETH Zürich, Switzerland. We used the published data for new oxybarometric calculations. Titanite (sphene) trace element compositions were analyzed at the Göochron Laboratories, University of Göttingen, Germany. A ThermoScientific Element 2 sector field ICP-MS was coupled to a RESOLution S-155 (Resonetics) 193 nm excimer laser (CompexPro 102) equipped with a two-volume ablation cell (Laurin Technic). The sample cell was flushed with high purity He (600 ml/min), whereas Ar was employed as the plasma carrier gas (0.985 l/min). Single spot analyses were conducted with a laser beam diameter of 33 µm and a crater depth of approximately 10 µm. The laser was fired at a repetition rate of 5 Hz and at an energy density of ~ 2.5 J/cm^2 on the sample surface. Analyses were performed both on titanite cores and rims. NIST 612 glass was used as the primary reference material to calculate elemental concentrations and to correct for instrumental drift. Silicon (^{29}Si) was used as the internal standard for reference materials and unknowns, where we assumed an Si content of 14.3 wt% for titanite. This first step of data reduction was performed using the Iolite software (Paton et al. 2011) and the final concentrations were calculated by an in-house spreadsheet. Results of the LA-ICP-MS measurements are presented in the ESM 2.

Using the EPMA and LA-ICP-MS compositional data, we then employed commonly used mineral ± melt thermometers, barometers, oxybarometers and chemometers as detailed in the ESM 1 (those of Watson and Harrison 1983; Andersen and Lindsley 1985; Holland and Blundy 1994; Anderson and Smith 1995; Ferry and Watson 2007; Anderson et al. 2008; Ghiorso and Evans 2008; Hayden et al. 2008; Ridolfi et al. 2010; Ridolfi and Renzulli 2012; Krawczynski et al. 2012; Waters and Lange 2015; Mutch et al. 2016; Putirka 2016; Arató and Audétat 2017a, b, c; Erdmann et al. 2019; Loucks et al. 2020; Ridolfi 2021; Crisp and Berry 2022; Higgins et al. 2022; Médard and Le Pennec 2022). The state of equilibrium between phases was evaluated by textural investigation and/or geochemical tests. The input data and the uncertainties of the results for each method are summarized in the ESM 1.

Results

Plagioclase

Plagioclase makes up 5 to 11 vol% of the studied samples of the Ee5/1–56 and Ee5/2–32 units respectively, and 7 vol% of the Ee5/1–50 unit (Table 1). Crystals range in size from 50 to 3500 µm in length. In the Ee5/1–56 and Ee5/2–32 pumice, i.e., in the youngest and the oldest investigated eruption products, plagioclase macrocrysts show often medium-to-coarse grained spongy cellular texture and oscillatory zoning in their interiors overgrown by 10–200 µm thick, typically euhedral and inclusion-free outermost rim (Fig. 2b–c). Amphibole and biotite as well as titanite, apatite, or zircon commonly form inclusions. In contrast, plagioclase crystals in the Ee5/1–50 pumices do not have spongy texture, they are inclusion-free to inclusion-poor (Fig. 2f). They show normal zoning occasionally with oscillatory zoned core without evidence of resorption. Inclusions of amphibole, biotite and the accessory minerals occur rarely. Amphibole inclusions are less common than in plagioclase from the Ee5/1–56 and Ee5/2–32 pumice and can be found mostly near the crystal rims.

Plagioclase cores and rims of each investigated explosive eruption unit show a relatively restricted compositional range (Figs. 2 and 3). In eruption units Ee5/2–32 and

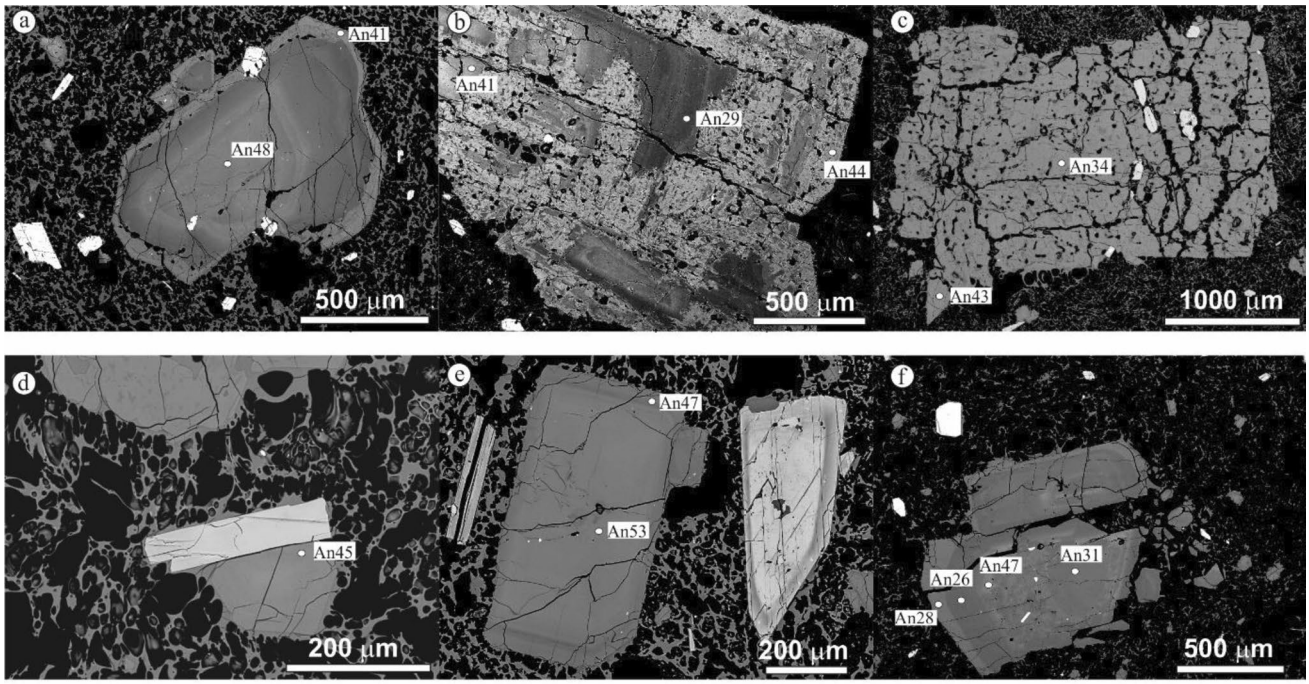

Fig. 2 Back-scattered electron images of the most frequent plagioclase types in **a–e** the Ee5/2–32 and the Ee5/1–56 eruption units; and **f** in the Ee5/1–50 unit. **a** Plagioclase macrocryst with oscillatory normal zoning at the interior overgrown by a more calcic thin rim. **b–c** Large, spongy textured plagioclase macrocrysts with amphibole and biotite inclusions occurring typically in these eruption units. **d** Coexisting amphibole and plagioclase. **e** Normal zoned plagioclase and reverse zoned amphibole. **f** Plagioclase macrocryst with biotite inclusions in the core. An indicates anorthite end-member (in mol%)

Ee5/1–56, the majority of plagioclase cores and rims have an An content between ~ 40 and 50 mol% with few core compositions extending to > 60 mol%. The FeO content varies between 0.1 and 0.4 wt%, showing a slightly positive correlation with An content (Fig. 3f). The rim composition is relatively homogeneous with An = 40–50 mol% and 0.2–0.3 wt% FeO content. In eruption unit Ee5/1–50, plagioclase core and rim compositions are significantly more evolved than in the other two eruption units, with An content mostly between 20 and 30 mol% (Fig. 3b, e). Their FeO content is between 0.1 and 0.4 wt% (Fig. 3e). Comparison with plagioclase from the older lava dome dacite can be found in the Table S2.

Amphibole

Amphibole is the most common mafic mineral phase in the studied samples, constituting 3–6 vol% (Table 1) in the pumices of the Ee5/1–56 and Ee5/2–32 units and ~ 1 vol% (Table 1) in the studied pumices of the Ee5/1–50 unit. Most of the crystals have euhedral shape, although they show various zoning types, i.e., complex normal (Fig. 4b, f), complex reverse (Fig. 4a, h), oscillatory (Fig. 4e, i), complex patchy (Fig. 4d) zoning, but also homogeneous crystals occur (Fig. 4c). Most commonly they are normally zoned with irregular resorbed, and occasionally patchy cores and thin, euhedral outer rims (Fig. 4b). In the Ee5/1–56 and the Ee5/2–32 pumices, i.e., in the oldest and the youngest investigated explosive eruption products, the amphibole cores often show coarse, vermicular resorption structure (Fig. 4a, d, h). In the Ee5/1–50 pumice, amphibole crystals equally show normal, occasionally slightly oscillatory zoned cores with resorbed margins overgrown by thin euhedral rims (Fig. 4f), and homogeneous, unzoned crystals often intergrown with biotite (Fig. 4g). Amphibole coexists with plagioclase either as inclusions or in intergrowth (Figs. 2a, c, d and 4c).

In contrast to the plagioclase, amphibole shows significant compositional variation in each investigated explosive eruption unit, often in single crystals (Fig. 4). Crystal composition is classified as magnesio-hornblende and pargasite/Mg-hastingsite based on the IMA classification scheme as described by Hawthorne et al. (2012) and Locock (2014) (Fig. S2). The compositional variation is illustrated in the Al_2O_3 vs. MgO diagram (Fig. 5), where five main groups can be distinguished: (1) low-Al, low-Mg amphibole (Al_2O_3 = 6.0–9.5 wt%, MgO < 14 wt%; Fig. 5), which forms mostly cores of reverse zoned crystals (Fig. 4a) and homogeneous macrocrysts often with biotite inclusions (Fig. 4d, g). They are relatively rare except for the Ee5/1–50

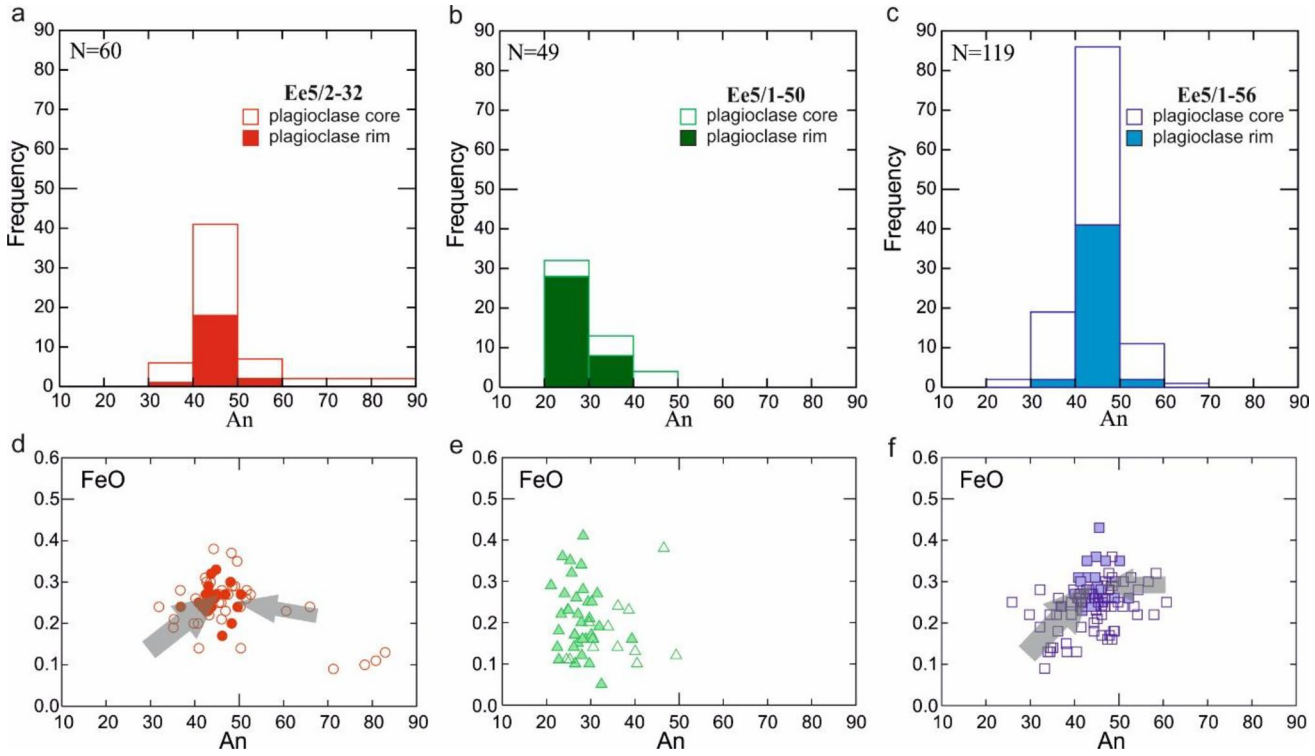

Fig. 3 Plagioclase An contents of the studied explosive eruption units. Plagioclase in the **a** Ee5/2–32 and **c** Ee5/1–56 units has closely comparable compositional maxima and compositional range, whereas plagioclase in the **b** Ee5/1–50 pumice have considerably more evolved composition. Arrows show the core-rim directions in the plagioclase crystals in pumices from the Ee5/1–56 and Ee5/2–32 units

pumices. Noteworthy, they have also elevated MnO content (MnO > 0.4 wt%). (2) High-Al, high-Mg (Al_2O_3 > 9 wt%, MgO > 16 wt%) amphibole (Figs. 4b, e, h, i and 5), which are irregularly resorbed, occasionally oscillatory cores of normal zoned macrocrysts. These crystals have typically low MnO (< 0.2 wt%). They are present only in the Ee5/1–56 and Ee5/2–32 pumices. (3) Low-Al, high-Mg amphibole, which has a unique, distinct compositional group (Al_2O_3 = 5–7 wt%, MgO = 19–21 wt%; Figs. 4f and 5). Remarkably, these amphiboles are characterized by high Cr_2O_3 content (0.3–1.3 wt%), while all the other amphibole types have Cr_2O_3 < 0.3 wt%. They occur exclusively in the pumices of the Ee5/1–50 unit and form the irregularly resorbed core of normal zoned macrocrysts (Figs. 4f and 5). Occasionally, they show slight oscillatory zoning. (4) High-Al, moderate-Mg amphibole (transitional type, Al_2O_3 = 9.5–11.5 wt%, MgO = 13–16 wt%; Figs. 4b, c and 5), which typically represents the rim composition of the macrocrysts in the Ee5/1–56 and Ee5/2–32 pumices and not found in the Ee5/1–50 pumices. (5) Low-Al, moderate-Mg amphibole (transitional type, Al_2O_3 = 7.5–9.0 wt%, MgO = 14–16 wt%), which forms rim of macrocrysts exclusively in the Ee5/1–50 pumices (Fig. 4f). The group (1) amphibole can be found also in the older lava dome samples (Kiss et al. 2014), whereas all the other amphibole groups differ from those found in the lava dome rocks (Fig. S3). Transect line profiles of amphibole crystals are in the ESM 2 and in Fig. S4.

Fe-Ti oxides

Ti-magnetite and ilmenite are both 50–200 µm in size and have a dominant rounded shape with glass embayments, indicating partial resorption (Fig. 6). Occasionally, they host apatite or biotite inclusions. Most of the crystals are embedded in the matrix, as observed in thin section and as shown by attached glass rims around Fe-Ti oxide grain separates. Noteworthy, the attached glass as well as the glass embayments have compositions slightly enriched in Fe and Ti, most probably caused by the rapid diffusion of these elements. Both BSE images and microprobe traverse analyses confirm homogeneous composition of the titanomagnetite and ilmenite crystals (Fig. 6, Fig. S5, ESM 2). As for plagioclase and amphibole, the calculated Fe-Ti oxide end-member compositions are closely comparable for crystals in the Ee5/2–32 and Ee5/1–56 units, but distinct for crystals in the Ee5/1–50 pumice. Titanomagnetite and ilmenite from the Ee5/1–56 and the Ee5/2–32 units have compositions with 12–18 mol% ulvöspinel (Usp) and 78–84 mol% ilmenite (Ilm), respectively, while in the Ee5/1–50 unit a slightly lower Usp (10.0–16.5 mol%) and significantly lower

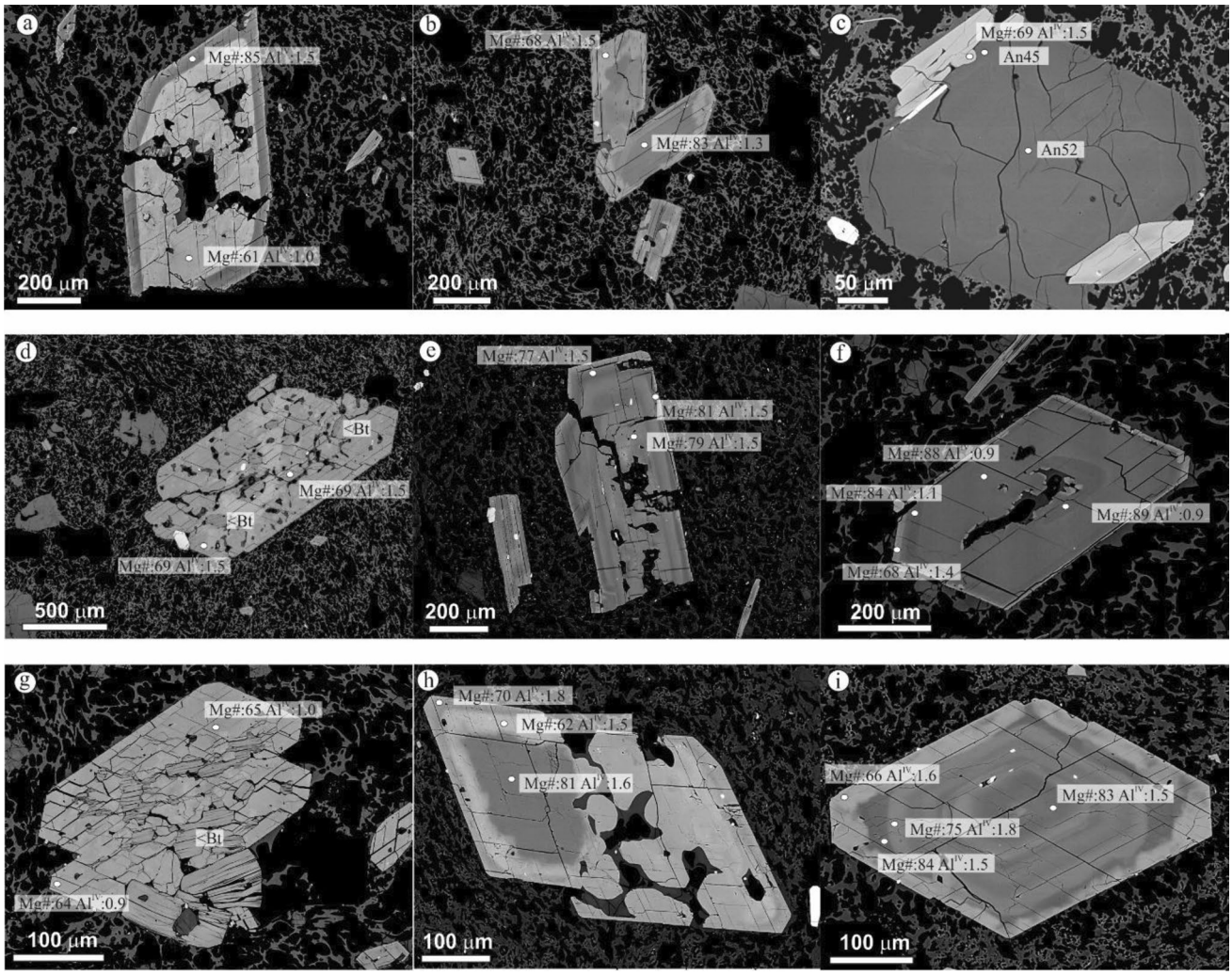

Fig. 4 Back-scattered electron images of characteristic amphibole types. **a** Low-Al, low-Mg patchy core in reverse zoned amphibole. The rim has high-Mg amphibole composition. **b** Normal zoned amphibole: high-Mg core with irregular, resorbed margin overgrown by an amphibole of transitional composition. **c** Amphibole with transitional composition coexistent with plagioclase. **d** Unzoned, spongy, patchy amphibole with transitional composition. **e** Oscillatory zoned amphibole with high-Mg amphibole composition and transitional type rim. **f** Normal zoned crystal with slightly patchy inner zone with low-Al, high-Mg amphibole composition and thin overgrowth of lower Mg and higher Al composition. **g** Unzoned low-Al, low-Mg amphibole intergrown with biotite. **h** Complexly zoned amphibole crystal with high-Mg, high-Al core showing irregular margin overgrown by a low-Mg amphibole zone and an outer rim of transitional composition. **i** Oscillatory zoned amphibole with high-Al, high-Mg core and transitional type outer rim. **a**, **b**, **d**, **e** Amphiboles are from the Ee5/1–56 pumice samples; **f**–**g** Typical amphibole types in the Ee5/1–50 pumice; **c**, **h**, **i** Amphiboles are from the Ee5/2–32 pumice samples

Ilm components (70–75 mol%) are observed. Furthermore, Ti-magnetite of the Ee5/1–50 pumice contains less V_2O_3 (0.12–0.35 wt%) than crystals in the other two eruption units, which have V_2O_3 between 0.2 and 0.5 wt%.

Zircon

Zircon crystals are euhedral to anhedral, oscillatory zoned crystals, having a maximum size of 300 µm. They rarely enclose apatite and/or opaque minerals in the core. Zircon commonly forms euhedral inclusions within amphibole and plagioclase crystals or appears in the groundmass. Their trace element compositions were presented by Lukács et al. (2021). In the three studied eruption units, zircon shows very similar texture and composition. Zircon Hf content is in the range from 9200 to 10,700 ppm, Yb/Dy varies between 5 and 8, whereas Ce, Th, and U concentrations are 30–90 ppm, 200–1400 ppm, and 400–2000 ppm (Th/U = 0.5–1.0), respectively (ESM 2). The chondrite-normalized rare earth element patterns show a slightly negative Eu-anomaly (Eu/Eu* = 0.60–0.85).

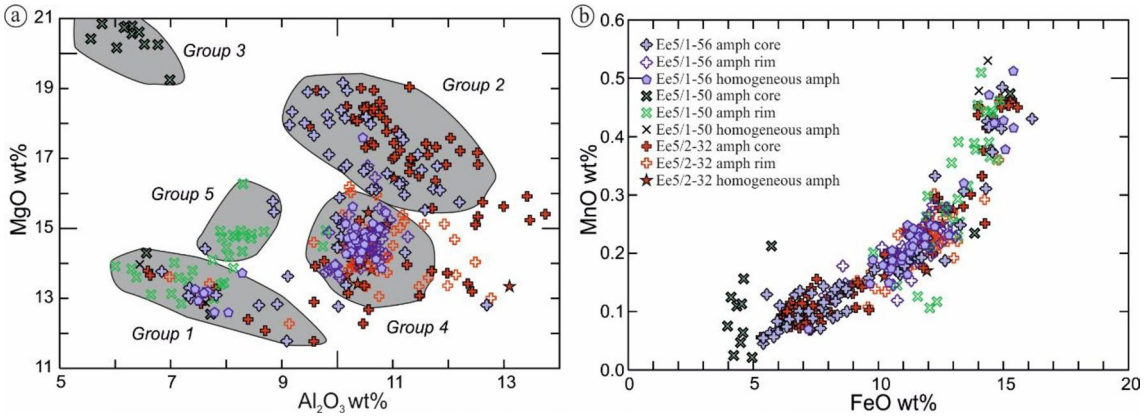

Fig. 5 Variation of amphibole chemical compositions (core and rim) of the studied pumice samples. The defined amphibole groups are indicated by grey areas: Group 1: Low-Al, low-Mg amphibole (Al_2O_3 = 6.0–9.5 wt%, MgO < 14 wt%); Group 2: High-Al, high-Mg (Al_2O_3 > 9 wt%, MgO > 16 wt%); Group 3: Low-Al, high-Mg amphibole (Al_2O_3 = 5–7 wt%, MgO = 19–21 wt%); these amphibole groups represent crystal cores. Group 4: High-Al, moderate-Mg amphibole (transitional type, Al_2O_3 = 9.5–11.5 wt%, MgO = 13–16 wt%); Group 5: Low-Al, moderate-Mg amphibole (transitional type, Al_2O_3 = 7.5–9.0 wt%, MgO = 14–16 wt%; these latter two amphibole groups are found as crystal rim and microcrysts

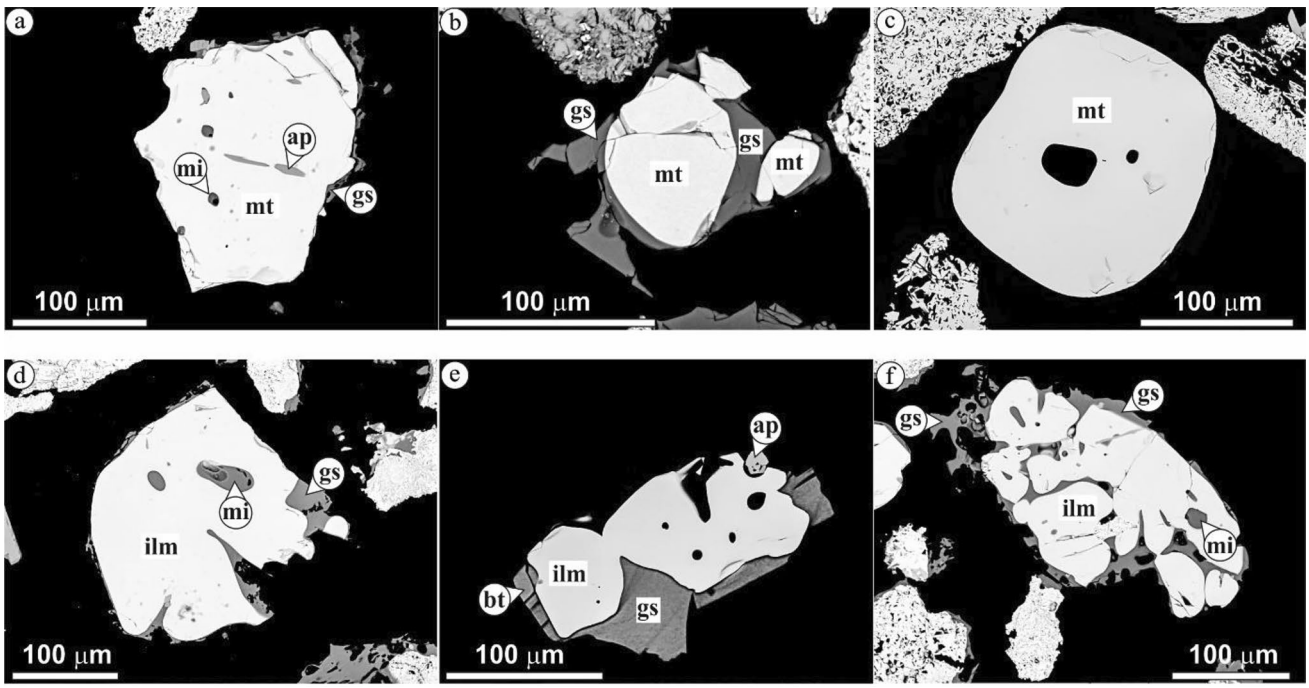

Fig. 6 Back-scattered electron (BSE) images of titanomagnetite (**a**–**c**) and ilmenite (**d**–**f**) crystals separated from the Ee5/2–32 (**a**–**b**, **d**, **f**) and the Ea5/1–56 (**c**, **e**) eruption units. Note the rounded, strongly resorbed crystals with homogeneous compositions. Abbreviations: *ap* apatite, *bt* biotite, *gs* glass, *mi* silicate melt inclusion, *mt* titanomagnetite, *ilm* ilmenite

Titanite

Titanite is always present in the Ciomadul dacites but occur in various amounts. In the Ee5/2–32 and Ee5/1–56 eruption units, titanite is particularly rare (< 0.1 vol%), found mostly in the heavy mineral separates and is typically < 450 μm in size. It most commonly forms inclusions in low-Al, low-Mg amphibole. In the Ee5/1–50 pyroclastic unit, titanite is also rare (< 0.5 vol%), forming mesocrysts with sizes of up to 750 μm. It is usually euhedral, forming single crystals in the groundmass, inclusions in amphibole or intergrown with amphibole. The zoning is similar to the other two units, but the resorption boundary between the core and rim is stronger (Fig. S7).

Titanites of the three studied eruption units have remarkably uniform composition. Their Al_2O_3 content varies between 1.2 and 1.4 wt%, whereas their Fe_2O_3 content is between 1.3 and 1.6 wt%. Most crystals show composite zoning patterns (Fig. S7), although they do not coincide with significant variation in major elements, but rather in rare earth elements. In general, oscillatory zoned crystal cores have less Fe and REE than the rim. On the other hand, a large variation in REE content is observed with a total rare earth element abundance from 10,000 to 18,000 ppm. The chondrite normalized rare earth element patterns are characterized by light REE-enrichment with respect to heavy REE ($Ce/Yb_N = 4.5–10.5$) with a slight negative Eu-anomaly ($Eu/Eu^* = 0.75–0.90$).

Glass

Glass composition was determined to complete the existing data set for the glassy matrix (which has up to 14 vol% microlites in the Ee5/2–32 and Ee5/1–56 pumice and 1–2% in the Ee5/1–50 pumice), for glassy silicate melt inclusions in amphibole and plagioclase, and for irregular, vermicular glass embayments in amphibole and Fe-Ti oxide crystals. In case of glassy matrix, measurements were performed in microlite free spots, usually next to crystal rims. The new results are interpreted with previously published data (Karátson et al. 2016; Laumonier et al. 2019; Harangi et al. 2020). The matrix glass and melt inclusion compositions in the Ee5/1–50 pumices have similar and fairly homogeneous composition between $SiO_2 = 75.0–76.5$ wt% and $Al_2O_3 = 13.5–14.5$ wt% in anhydrous basis. In contrary, glasses from the two other units have a wider compositional range ($SiO_2 = 70.5–73.5$ wt% and $Al_2O_3 = 14.2–16.8$ wt%) that strikingly differs from the Ee5/1–50 glasses as already pointed out already by Vinkler et al. (2007), Karátson et al. (2016) and Harangi et al. (2020). This wide compositional range is partly due to the different compositions of glass inclusions of various mineral phases and avoiding the more evolved and less evolved glass inclusion data, the glasses are characterized with more homogeneous $SiO_2 = 71.5–72.5$ wt% and $Al_2O_3 = 15.5–16.0$ wt% compositions. The estimated H_2O content of the glasses (calculated by difference method; Devine et al. 1995) varies significantly, between 0.5 and 7 wt%.

Discussion

Origin of the crystal cargo

The Ciomadul dacitic pumices contain very similar mineral assemblage, however, their chemical compositions, particularly those of amphibole show a great range. Remarkably, the compositional variation of amphibole in the 56–32 ka Ciomadul pumices is one of the largest compared to several examples of similar andesitic to dacitic systems (Fig. 7; e.g., Fish Canyon Tuff, Colorado, USA, Bachmann et al. 2002; Savo, Solomon Islands, Smith 2014; Mt St. Helens, Washington, USA, Thornber et al. 2008; Shiveluch, Kamchatka, Russia, Goltz et al. 2020;

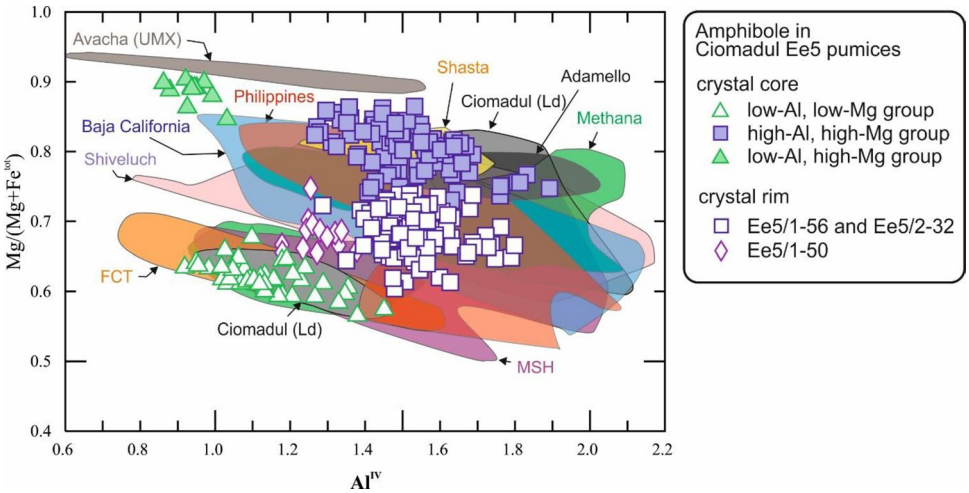

Fig. 7 Tetrahedral Al (Al^{IV}) vs. Mg# [$Mg/(Mg+Fe^{tot})$] compositions for the Ciomadul amphibole groups. For comparison, amphibole compositional fields for several andesitic-dacitic volcanic rocks are also presented. Ciomadul (Ld = lava domes, Kiss et al. 2014); FCT: Fish Canyon Tuff (Bachmann et al. 2002); MSH: Mt St. Helens (Thornber et al. 2008); Shiveluch (Kamchatka, Goltz et al. 2020; Gorbach et al. 2020); Shasta (California, USA, Grove et al. 2003); Methana (Greece, Popa et al. 2020); Philippines and Baja California (Ribeiro et al. 2016). In addition, amphibole cumulate composition from Adamello (Tiepolo et al. 2011) are shown as it represents high pressure and high temperature phases and the amphibole compositional data field for ultramafic xenoliths from Avacha, Kamchatka (Ionov 2010) are also indicated, which are similar to the unique low-Al, high-Mg amphiboles of the Ee5/1–50 unit

Gorbach et al. 2020; Longaví, Andean Southern Volcanic Zone, Central Chile, Rodríguez et al. 2007; Lamington, Papua New Guinea, Humphreys et al. 2019; Methana, Greece, Popa et al. 2020; Philippines and Baja California, Ribeiro et al. 2016). Kiss et al. (2014) pointed out that low-Al, low-Mg amphiboles from the older Ciomadul lava domes represent a shallow felsic magma reservoir that existed for several 100's of thousand years before eruptions occurred (Lukács et al. 2021). Reactivation of this highly crystalline mush occurred repeatedly by magma recharges transporting high-Mg amphibole as well as olivine and clinopyroxene to the felsic magma storage. Comparing to the lava dome rocks, a striking difference in the explosive volcanic products studied in this paper is that no olivine and clinopyroxene are found with exception for sporadic mafic crystal clots with amphibole and more notably, the amphibole compositional range is different. Thus, the following main components of the Ciomadul magma reservoir system have to be considered as playing role in the magma evolution and eruption trigger: (1) long-standing evolved felsic crystal mush body in the shallow crust; (2) recharge magmas and (3) post-recharge, pre-eruption magma batch. Each of these magmatic components could have its own characteristics reflected in the mineral chemistry and texture. Therefore, first, we interpret the origin of the crystal cargo, followed by a careful evaluation of the crystallization conditions in order to reconstruct the nature and dynamics of the trans-crustal magma storage system.

In the three studied explosive eruption units, five compositionally different amphibole types have been identified. Normal zonation is the most common (characteristic of ~ 55% relative abundance within the amphibole crystals in the Ee5/1–56 and Ee5/2–32 pumices and ~ 44% in the Ee5/1–50 pumice), where the inner crystal cores are Mg- and Al-rich (MgO > 16 wt%, Al_2O_3 = 10–12 wt%) in case of the Ee5/1–56 and Ee5/2–32 pumices, however, Mg-rich and Al-poor (MgO = 19–21 wt%, Al_2O_3 = 6–7 wt%) in case of the Ee5/1–50 pumice. In all eruption products, these crystal cores are characterized by slight oscillatory zoning or patchy textures and have irregularly resorbed outer margins and glass embayments (Fig. 4b, e, f, h, i). Occasionally, the high-Mg, high-Al amphibole forms mafic crystal clots accompanied with ortho- and clinopyroxene, while plagioclase is notably absent from this assemblage (Cserép et al. in prep). These high-Mg amphiboles are clearly not in equilibrium with the dacitic magma and could have been transported into the felsic magma reservoir via more mafic recharge magma. Thus, they are classified as antecrysts, which provide insights into the deeper part of the magma reservoir. Compared to the Mg-rich amphibole from older dome-forming eruptions (Kiss et al. 2014), they have higher Mg and lower Al content suggesting distinct type of recharge magma.

The low-Al, low-Mg amphiboles (Al_2O_3 = 6–9 wt%, MgO < 14 wt%; Ee5/1–56 and Ee5/2–32: ~ 15%; Ee5/1–50: ~ 24% of the total amphibole crystals) are present in all the three studied eruption units, where they occur in notably lower amounts than in the older lava dome rocks (Kiss et al. 2014). This amphibole type occurs as large unzoned, strongly resorbed (spongy) macrocrysts typically with biotite inclusions (Fig. 4d, e) and forms also cores of reversely zoned crystals (Fig. 4a, g). They occasionally form also felsic crystal clots with large plagioclase and biotite, apatite, Fe-Ti oxides, titanite and zircon. In the older lava dome rocks, these crystal clusters are associated with quartz and K-feldspar, but these two phases have not been identified in the studied pumices. The low-Al, low-Mg amphibole has the same chemical composition as the hornblende group in the lava dome rocks (Fig. 7) and is interpreted to represent the pre-recharge, shallow felsic crystal mush (Kiss et al. 2014). Their strongly resorbed appearance indicates that they are not in equilibrium with the erupted magma. Therefore, they are considered also as antecrysts, i.e., they crystallized in the same magma reservoir but from different melt along with biotite, plagioclase, apatite, titanite and zircon and possibly also with quartz and K-feldspar, well before the eruptions. We use their compositions, along with the coexisting phases, to determine the intensive parameters of the long-lived shallow magma reservoir.

The high-Al, moderate-Mg amphibole type (Al_2O_3 = 10–12 wt%, MgO = 14–16 wt%; ~ 30% of the total amphibole crystals in the Ee5/1–56 and Ee5/2–32) and the low-Al, moderate-Mg amphibole (Al_2O_3 = 8–9 wt%, MgO = 14–15 wt%; Ee5/1–50: ~ 32%) have transitional compositional character. They mostly represent the thin rim on the normal and reverse zoned crystals (Fig. 4e, f), although they occur also as homogeneous, euhedral microphenocrysts. These amphiboles often form equilibrium pairs with plagioclases (Fig. 4c). The narrow rim (Ee5/2–32: 6–71 µm; Ee5/1–50: 6–45 µm; Ee5/1–56: 15–65 µm) and euhedral shape suggest that overgrowth crystallization occurred after the rejuvenation event in equilibrium with the host melt represented by the groundmass glass. Using compositions of this assemblage, constraints on intensive parameters immediately before the eruption can be obtained. Fe-Ti oxides in particular re-equilibrate rapidly, within hours to days (Venezky and Rutherford 1999; Morgado et al. 2019; Prissel et al. 2020; Hou et al. 2021) and they therefore typically record this post-recharge to syn-eruptive condition.

In the Ciomadul pumices, plagioclase shows much less compositional variation compared to the amphibole population. In the Ee5/1–56 and Ee5/2–32 units, they range in An between 30 and 60 mol%, although the rim compositions are narrow, between 40 and 50 mol%. Microphenocrysts

(micro- and mesocrysts), which are often intergrown with transitional type amphibole have the same composition as the macrocryst rims. Thus, they may have crystallized from the post-recharge hybrid magma, and their compositions are therefore used as an equilibrium pair with the transitional type (high-Al, moderate-Mg) amphibole for thermobarometric estimation (ESM 1, Fig. S8). A characteristic plagioclase type (~25% of the total plagioclase crystals) in these units are large (usually > 1 mm) macrocrysts with spongy-cellular texture (e.g., Fig. 2b, c). They have An = 25–35 mol% composition (used with the low-Al, low-Mg amphibole for thermobarometric estimation; ESM 1, Fig. S8) similar to plagioclase of the felsic crystal clots in the older lava domes (Kiss et al. 2014). Therefore, we interpret them as antecrysts derived from the felsic crystal mush, which were partly resorbed during entrainment and magma recharge. An overgrowth with higher An (An = 40–50 mol%) and FeO composition (Fig. 3) formed on these crystals prior to eruption.

There is no clear evidence that the recharge magma transported plagioclase into the felsic magma reservoir as shown for instance by Popa et al. (2020) in case of the Methana volcanic rocks. The mafic crystal clots in the Ciomadul pumice do not contain plagioclase with high-Ca cores, typical of early-formed plagioclases in arc-magmas (e.g., Melekhova et al. 2015; Klaver et al. 2017; Popa et al. 2020), except for a single case in the Ee5/2–32 unit. The suppression of plagioclase stability in the deep mafic magma reservoir can be explained by hydrous conditions (> 6 wt%; Pichavant and Macdonald 2007; Melekhova et al. 2015). Nevertheless, the normal zoned plagioclase crystal cores with An = 48–60 mol% (e.g., Fig. 2a, e) might have crystallized from the recharge magma en route to the shallow magma reservoir and then, they were also overgrown by the typical An = 40–50 mol% post-recharge rim.

Plagioclase from pumice of the Ee5/1–50 unit has distinct composition as was shown already by Harangi et al. (2020). In these rocks, no sieve-textured macrocrysts occur. The crystals are inclusion-free or -poor, showing only subtle inner oscillatory compositional variation (crystal cores: An = 30–50 mol%; crystal rims: An = 20–30 mol%). This indicates that recharge affected another, more evolved part of the crystal mush and that the recharge melt did not cause much compositional variation of the melt fraction.

The groundmass glass of the studied pumices potentially represents the post-recharge melt composition of the erupted magmas. It formed by hybridization of melt from the felsic crystal mush and melt from the recharge magma as well as melt derived from the remelted crystal assemblage. The groundmass glass contains various plagioclase microlites, particularly in the Ee5/1–56 and Ee5/2–32 samples that formed during magma ascent (e.g., Andrews and Gardner 2010) and can obscure the original glass composition. Taking into account only the microlite-free glass data, glasses have relatively homogeneous, evolved composition, which can reflect the melt fraction of the erupted magma where the post-recharge crystal phases were equilibrated. This melt composition strikingly differs in the Ee5/1–56, Ee5/2–32 and the Ee5/1–50 samples, respectively (SiO_2 = 71.5–72.5 wt%, Al_2O_3 = 15.5–16.0 wt% and SiO_2 = 75.0–76.5 wt%, Al_2O_3 = 13.5–14.5 wt% in anhydrous basis) and implies that distinct parts of the shallow magma reservoir were potentially affected during the reactivation.

Intensive parameters of Ciomadul's magma system

A large number of potential thermobarometers, oxygen barometers, and chemometers exist (e.g., Putirka 2008; Wieser et al. 2022a, b), yet they commonly provide disparate results, and many have high uncertainties. This is primarily due to the experimental condition used for calibration and the applied regression strategy (linear vs. non-linear). Thus, in the following sections, we critically discuss the results obtained by various calibrations (ESM 1) and present our best estimates for the Ciomadul magma system. We also directly consider constraints from phase equilibrium experiments on dacitic magmas from Scaillet and Evans (1999), Pichavant et al. (2002), Prouteau and Scaillet (2003), and Costa et al. (2004).

Pressure

Crystallization pressure is an important parameter since it provides information about the depth of magma storage and the architecture of trans-crustal magma systems. The Al content of amphibole is pressure-sensitive (Hammarstrom and Zen 1986; Hollister et al. 1987; Johnson and Rutherford 1989a; Schmidt 1992; Anderson and Smith 1995), where increasing pressure favors Al-Tschermak substitution. In the Ciomadul pumice, amphibole Al^{IV} (tetrahedral Al) and Al^{VI} (octahedral Al) correlate with each other (Fig. S9). The high-Al, high-Mg and the transitional type amphiboles have typically variable, high Al^{VI}, implying crystallization at various pressures, although temperature (Blundy and Holland 1990) and particularly magma composition also, and probably more sensitively, control the Al content in the amphibole (Erdmann et al. 2014; Kiss et al. 2014; Putirka 2016). Amphibole barometers without additional constraints on other intensive parameters therefore have significant uncertainties (Table S3), and they cannot resolve crustal magma storage depths. Yet, Al-in-amphibole barometers calibrated for specific mineral assemblages, granitic magma compositions, and near-solidus temperatures (≤ 800 °C)—as those of Johnson and Rutherford (1989a), Mutch et al. (2016) and Médard and Le Pennec (2022)—may yield reliable constraints. To be applicable, the barometers

require an assemblage of amphibole, plagioclase, biotite, quartz, K-feldspar, ilmenite/titanite, magnetite, and apatite and a melt composition close to the haplogranitic solidus. The studied Ciomadul pumice samples lack quartz and K-feldspar in their assemblage. The required barometer mineral assemblage is, however, observed in the 160–90 ka lava dome rocks of Ciomadul, where it is interpreted to represent low-temperature crystal mush (Kiss et al. 2014; Laumonier et al. 2019), and pressure therefore can be estimated for the dome rocks and their crystal mush fragments. In the studied pumices, the composition of low-Al, low-Mg amphibole and other co-existing phases is notably similar to those found in the lava dome rocks (Fig. S3). This could indicate that the crystal mush fragments were close to quartz and alkali feldspar saturation and quartz and alkali feldspar were consumed during mush rejuvenation by magma recharge. We therefore cautiously apply the Al-in-amphibole barometers to the low-Al amphibole compositions of the Ciomadul pumice, and will further discuss the possible limitations of the pressure estimate.

The calculated pressure values for the low-Al, low-Mg amphibole are between 200 and 330 MPa using the equation given by Mutch et al. (2016), between 160 and 295 MPa using the calibration of Médard and Le Pennec (2022), and between 241 and 296 MPa using the barometer of Anderson et al. (2008). The barometers of Ridolfi et al. (2010), Ridolfi and Renzulli (2012) and Higgins et al. (2022) were calibrated without consideration of a specific magma composition or equilibration assemblage, but differ from each other in the applied regression strategy as well as the considered experimental data set. The former two barometers calculate pressures of < 130 MPa, whereas the latter one gives 300–450 MPa. Following others (e.g., Erdmann et al. 2014; Kiss et al. 2014; Putirka 2016), we interpret these results as relative under- and overestimates for the crystallization pressure of the low-Al, low-Mg amphibole, but highlight that all calculated values concur within the uncertainty of the estimates.

Titanite is a common mineral in the Ciomadul dacites and is considered to have crystallized in the evolved felsic crystal mush (Kiss et al. 2014). It has a relatively low Al_2O_3 content showing limited variance (~ 1.4–1.6 wt%). Applying the Al-in-titanite barometry of Erdmann et al. (2019), a narrow pressure range between 190 and 215 MPa was obtained. As for the near-solidus amphibole barometers, the titanite barometer should only be applied to assemblages comprising quartz and K-feldspar. However, as we argued above, the felsic crystal mush presumably contained these mineral phases before the magma recharge. Titanite is a characteristic low-temperature crystal mush mineral and its barometer can provide reliable results for the Ciomadul rocks. Notably, the calculated pressure range fits well within uncertainties with the crystallization pressures estimated using the Anderson et al. (2008), Mutch et al. (2016), and Médard and Le Pennec (2022) equations for the low-Al, low-Mg amphibole population. Therefore, we conclude that a felsic crystal mush body, where low-Al and low-Mg amphibole and titanite were stable resided in a pressure range between 200 and 300 MPa (Fig. 8d) what is consistent also with experimental data (Fig. 8b). Using a 2.5 g/cm^3 average density value for the upper crust, the calculated amphibole and titanite pressure range corresponds to a depth of ~ 8–12 km, which is consistent with the location of the presumed upper crustal magma reservoir inferred from an electrical conductivity anomaly beneath Ciomadul (Harangi et al. 2015b; Laumonier et al. 2019).

In contrast to the low-Al, low-Mg amphibole population, the crystallization pressure of the high-Al amphibole groups is difficult to constrain because of a lack of well-constrained experimentally determined compositions and the relatively large uncertainties of the applicable geobarometers (up to ± 160 MPa). The high-Al amphibole groups typically have higher octahedral and tetrahedral Al than the low-Al amphibole group (Fig. S9) and their octahedral and tetrahedral Al concentrations are positively correlated, suggesting crystallization at variable pressure, although melt composition could also be varied (Ridolfi et al. 2010; Krawczynski et al. 2012; Kiss et al. 2014). In case of the 133 ka Ciomadul Mic lava dome rocks, Kiss et al. (2014) pointed out (based on textural observations) that high-Al and high-Mg amphibole could have crystallized at low pressure from mafic magma (they form rim on low-Al, low-Mg amphibole core). In contrast, in the studied pumice, this amphibole type forms cores of the macro- and mesocrysts, often with resorbed outer boundaries. We interpret them as crystallization product from distinct magma, presumably at higher temperature and higher pressure, thus, they were transported by recharge magma from deeper zones into the shallow felsic magma reservoir. However, the machine learning method of Higgins et al. (2022) and the Ridolfi et al. (2010) geobarometer calculate pressure values, between 174 and 540 MPa, partly overlapping with that obtained for the felsic crystal mush body, although we note that these results need to be considered with caution.

The high-Al amphibole in the Ciomadul pumices has high Mg# (> 0.78), which is relatively rare in calc-alkaline magmas, but characteristic mostly of amphibole found in high-Mg andesites (e.g., Shasta, USA; Grove et al. 2003; Phillippines and Baja California; Ribeiro et al. 2016; Fig. 7), is interpreted to have crystallized from the recharge magmas prior to mixing with upper crustal crystal mush. Krawczynski et al. (2012) demonstrated experimentally that there is a narrow stability field where olivine and high-Mg amphibole may coexist in andesites and the Mg-value of the first appearing amphibole can be used to constrain pressure. There are petrological observations for the high-Mg

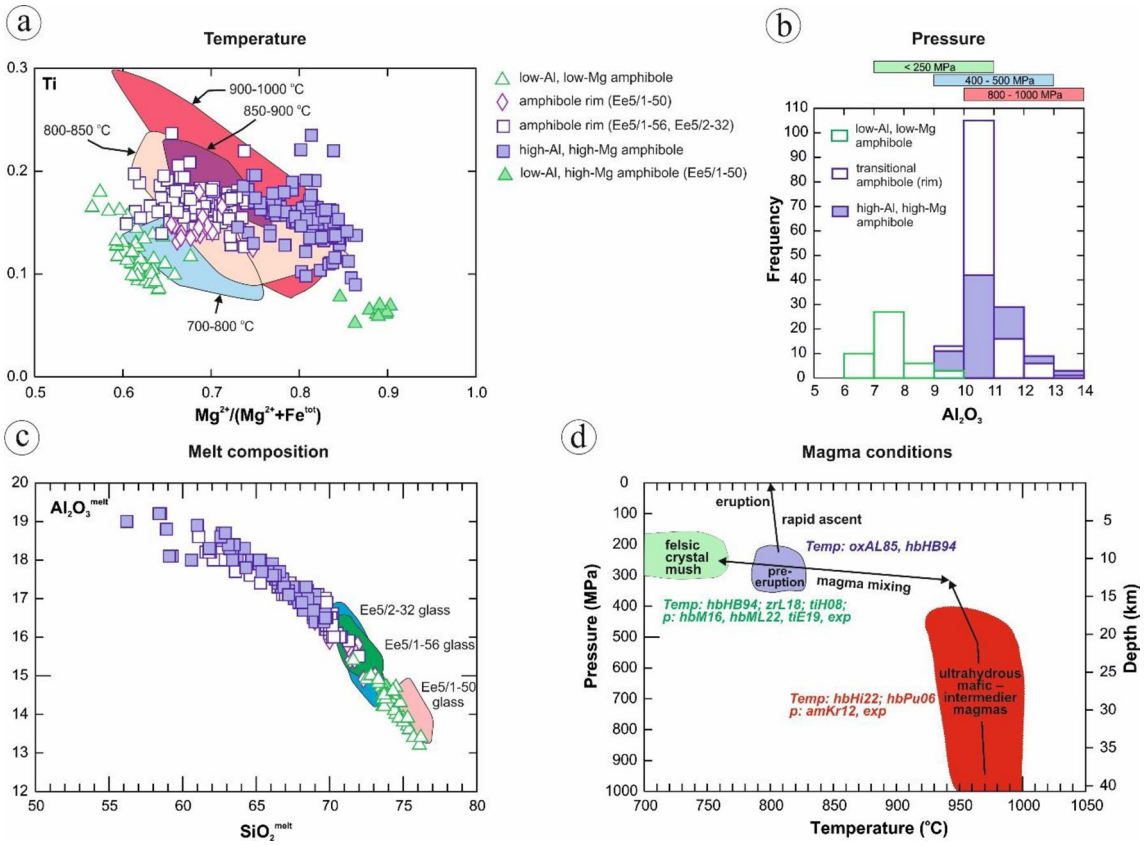

Fig. 8 Thermobarometric and chemometric results for the 56–30 ka Ciomadul magma system. **a** Comparison of amphibole composition from the Ciomadul pumices with experimental data of Scaillet and Evans (1999), Prouteau and Scaillet (2003), and Costa et al. (2004) for Ti vs. Mg# ($Mg^{2+}/Mg^{2+}+Fe^{tot}$) space. **b** Comparison of the Al_2O_3 content of the studied Ciomadul amphibole with the composition of amphibole crystallized over a range of pressure in the experiments of Scaillet and Evans (1999), Prouteau and Scaillet (2003), and Costa et al. (2004). **c** Chemometric results to constrain the melt composition in equilibrium with the amphibole compositions using the Higgins et al. (2022) method. Note the excellent fit with the glass data in the pumice. **d** Summary diagram for the estimated crystallization temperatures and pressures (hbHB94: amphibole-plagioclase thermometry by Holland and Blundy 1994; zrL20: zircon thermometry by Loucks et al. 2020; tiH08: Zr-in-titanite thermometry by Hayden et al. 2008; hbM16: hornblende barometry by Mutch et al. 2016; hbML22: Médard and LePennec 2022; tiE19: Al-in-titanite barometry by Erdmann et al. 2019; oxAL85: Fe-Ti oxide thermometry by Andersen and Lindsley 1985; hbHi22: amphibole thermometry and barometry by Higgins et al. 2022; hbPu16: amphibole thermometry by Putirka 2016; amKr12: amphibole Al^{VI} barometry by Krawczynski et al. 2012; exp: direct comparison of experimental data) to reconstruct the plumbing system and processes beneath Ciomadul during the youngest (56–30 ka), explosive eruption period

amphiboles in the studied Ciomadul pumices (e.g., mafic crystal cumulates with olivine or pyroxene in the core surrounded by amphibole corona and lacking plagioclase) indicating that they crystallized before plagioclase and coexisted with olivine, orthopyroxene, and clinopyroxene. Thus, the empirical geobarometer provided by Krawczynski et al. (2012) can be potentially applied to the Mg-rich amphibole compositions with Mg# between 0.74 and 0.84. The obtained pressure values are in the range of 400–570 MPa. It is noted that in the Ciomadul pumices, there are amphiboles with Mg# even higher than 0.84, but they are out of the calibration range.

In order to further constrain the pressure of the high-Al, high-Mg amphibole population in the Ciomadul pumices, we considered phase-equilibrium experiments, which fit the best with the conditions of the Ciomadul magmatic system (Scaillet and Evans 1999; Prouteau and Scaillet 2003; Costa et al. 2004). These experiments run between 200 and 1000 MPa, where high-Al_2O_3 (> 10 wt%) amphibole was exclusively produced at > 400 MPa (Fig. 8b), in equilibrium with ortho-and clinopyroxene, olivine or plagioclase. In addition, these amphiboles have compositions similar to the high-Mg amphiboles considered as high pressure (1000 MPa) cumulates found in hornblendites and hornblende gabbros of the Mt Mattoni section of the Adamello intrusive complex (Tiepolo et al. 2011; Fig. 7). In summary, we conclude that the high-Al, high-Mg amphibole group presumably formed between 400 and 1000 MPa (Fig. 8d), which corresponds to a depth range between 16 and 40 km (crust-mantle boundary zone beneath Ciomadul). Magmas

carrying these amphibole crystals ascended and intruded into the upper crustal felsic magma reservoir and remobilized a portion of the felsic crystal mush. Amphibole with high-Al and moderate-Mg composition (transitional type) is inferred to have crystallized at this stage just prior to eruption from a hybrid magma after mixing between the recharge magma and a smaller amount of the residing crystal-rich felsic magma. They form always rim of the macro- and mesocrysts as well as meso- and microcrysts, which occur occasionally with plagioclase. Applying the geobarometer of Médard and Le Pennec (2022), a little bit higher pressure values (300–400 MPa; Fig. S10) were obtained than for the crystal mush amphibole. Although, the results have to be accepted with caution, they could fit the environment where the magma mixing occurred.

In conclusion, the pressure estimates, although with relatively large uncertainty, indicate a magma reservoir system beneath Ciomadul with a prominent lower crustal hot zone and a mid-crustal, shallower felsic magma storage zone.

Temperature

Compositional variation of amphibole depends strongly on crystallization temperature (Blundy and Holland 1990; Holland and Blundy 1994; Bachmann et al. 2002). This is primarily recorded by the edenite and, to a lesser amount, by the Ti-Tschermak exchange. For the Ciomadul amphibole compositions, high regression coefficients of 0.93 and 0.88 were obtained for correlation between Al^{IV} and $(Na + K)^{A}$ and Al^{IV} and Ti, respectively, suggesting amphibole crystallization at a range of temperatures. However, determination of crystallization temperature is not straightforward as shown by variable temperature estimates from published amphibole thermometers (e.g., Blundy and Holland 1990; Holland and Blundy 1994; Anderson et al. 2008; Ridolfi et al. 2010; Ridolfi and Renzulli 2012; Molina et al. 2015; Putirka 2016; Ridolfi 2021; Higgins et al. 2022; ESM 1). The main reason for the variation is that the thermometers were calibrated on various sets of experimental data and with different regression methods (Higgins et al. 2022). A common feature to all amphibole thermometers is that they use experimental amphibole compositions that crystallized mostly at > 800 °C; therefore, they usually yield temperature overestimates for amphiboles formed < 800 °C (e.g., Ridolfi et al. 2010; Putirka 2016). However, amphibole-plagioclase thermometry of Holland and Blundy (1994) provides reliable results between 700 and 900 °C for calc-alkaline magmatic systems. An independent test of the reliability of the amphibole thermometry is the direct comparison with experimental results obtained for dacitic magmas similar to those of Ciomadul (e.g., Scaillet and Evans 1999; Prouteau and Scaillet 2003; Costa et al. 2004) in Fig. 8a.

Amphibole is often intergrown with plagioclase in the studied pumices, therefore amphibole-plagioclase thermometry (Blundy and Holland 1990; Holland and Blundy 1994; Anderson et al. 2008) is suitable to estimate the thermal condition of the Ciomadul magma reservoir. The thermometer can be applied to both the low-Al, low-Mg amphibole and low-An (25–30 mol%) plagioclase pairs as well as to the transitional amphibole and higher-An (40–50 mol%) plagioclase pairs, which represent the crystal mush and the pre-eruptive magma conditions. For the low-Al, low-Mg amphibole and low-An plagioclase pairs, both the edenite-richterite thermometer (which does not require quartz in the assemblage) and the edenite-tremolite thermometer (requiring the presence of quartz) were applied, calculating a temperature range between 680 and 760 °C. These estimates are in close agreement with the temperature estimates published by Kiss et al. (2014) for the 133 ka Ciomadul Mic lava dome rocks. Thus, this low-temperature range characterizes the shallow crustal felsic crystal mush. A similar temperature range (i.e. 700–800 °C) was calculated for amphibole from shallow, dacitic crystal-rich mush reservoirs that erupted the Fish Canyon Tuff (Bachmann et al. 2002), at Mt St Helens (Thornber et al. 2008), Savo (Smith 2014), Lamington (Humphreys et al. 2019) and Methana (Popa et al. 2020), among other eruption centers. In contrast, higher temperature values (typically 850–900 °C) are obtained for the low-Al, low-Mg amphibole population of Ciomadul pumices using the thermometer of Putirka (2016) equation and also by the thermometer of Higgins et al. (2022), which we consider as overestimates reflecting their higher temperature (> 800 °C) amphibole compositional calibration data set.

The low temperature (< 760 °C) magma storage of crystal mush in Ciomadul's shallow (at 8–12 km depth) plumbing system is corroborated by estimates using the zircon and titanite compositions and thermometry. Lukács et al. (2021) calculated temperature values of 670–730 °C with an uncertainty of ± 25 °C using the Ferry and Watson (2007) Ti-in-zircon thermometry at a Ti activity of 0.6 and Si activity of 1. These estimated temperature values are in agreement with those obtained using Zr-in-titanite thermometry (690–720 °C; Hayden et al. 2008) and this suggests crystallization presumably at or near the H_2O-saturated solidus. Trace element composition, notably the depletion in Zr in the low-Al amphibole from the older lava dome rocks (Kiss et al. 2014) indicates zircon fractionation before/during low-Al and low-Mg amphibole crystallization. The coeval amphibole and zircon crystallization is supported also by the wide range of Yb/Dy ratio in zircon. The calculated zircon saturation temperatures can be another constrain for the zircon crystallization. The Watson and Harrison (1983) and Crisp and Berry (2022) methods give similar result between 750 and 780 °C, which is considered as the maximum temperature for zircon crystallization. This is consistent with the

geochemical observation, i.e., zircon crystallization could start even before the onset of low-Al amphibole crystallization and could continue along with it down to the eutectic temperature. Thus, the upper crustal, highly crystalline felsic magma mush beneath Ciomadul before reactivation is inferred to have been at a temperature between 670 and 780 °C, but crystallization occurred mostly below 760 °C (Fig. 8d).

Crystallization temperature of the high-Al and high-Mg amphibole forming the cores of normally zoned phenocrysts can be estimated only using single-amphibole thermometry because they lack coexisting plagioclase. All amphibole-only thermometers (Ridolfi et al. 2010; Ridolfi and Renzulli 2012; Putirka 2016; Ridolfi 2021; Higgins et al. 2022) give temperature values above 880 °C (880–980 °C), suggesting that the amphibole crystallized from less evolved, hotter melt. This is consistent with the geobarometry results discussed in the previous section placing the origin of these magnesian amphiboles mostly to the lower crustal hot zone. The inference is also supported by phase equilibrium experiments on dacitic magmas (Scaillet and Evans 1999; Prouteau and Scaillet 2003; Costa et al. 2004), where the composition of the high-Mg amphiboles from the Ciomadul pumice overlaps with experimental amphibole produced between 850 and 1000 °C (Fig. 8a).

The amphibole crystals in the Ciomadul dacitic pumice have variable zoning patterns, but remarkably, they usually have euhedral shape and a narrow outer rim. The amphibole rims have similar chemical composition (Al_2O_3 = 10–11 wt%; Fig. 5) both on low- and high-Al cores. The crystal cores are therefore inferred to record crystallization at various stages and from compositionally different magmas prior to the recharge event, whereas the outer rims crystallized shortly prior and during eruption from variably mixed and equilibrated melts.

Fe-Ti oxides with fast re-equilibration behavior can be potentially used to constrain the final physicochemical condition in the magma reservoir prior to eruption and serve as independent check of the thermometry results for amphibole rim compositions. In each sample, we detected Ti-magnetite-ilmenite pairs in equilibrium as confirmed by the Bacon and Hirschmann (1988) test. Different temperatures were calculated using the Ghiorso and Evans (2008) and Andersen and Lindsley (1985) thermometers, respectively. In general, significantly lower temperatures were obtained by the Ghiorso and Evans (2008) geothermometer than by the Andersen and Lindsley (1985) method (Fig. S11). Average pre-eruptive temperatures, according to the calculations of the Ghiorso and Evans (2008) thermometer range between 720 and 745 °C, whereas the Andersen and Lindsley (1985) method yields calculated temperatures between 780 and 820 °C. Such a temperature difference (average Δ50–90 °C) between the results of the two thermometers is not unique. Similar differences were observed in the case of Pinatubo (previous thermobarometric studies: Pallister et al. 1996; Rutherford and Devine 1996), Mt St. Helens (Blundy et al. 2008), or the Fish Canyon Tuff (Whitney and Stormer 1985; Johnson and Rutherford 1989b) where the Ghiorso and Evans (2008) method always provides significantly lower temperatures (ca. Δ50–120 °C) than the Spencer and Lindsley (1981) or the Andersen and Lindsley (1985, 1988) thermometers. A common feature of all these volcanic systems, including Ciomadul, is that they had a relatively high oxidation state (ΔNNO > 1; see next section). In contrast, no differences in the temperature estimates were observed using these two methods in the case of Santorini (Cadoux et al. 2014) and the Bishop Tuff (Evans et al. 2016), which are characterized by comparatively reduced redox state (ΔNNO = − 0.9 to 0.5). Thus, it appears that the Ghiorso and Evans (2008) method potentially underestimates the pre-eruptive temperature of relatively oxidized magmas (cf. Loucks et al. 2018), whereas its results are consistent with those of the Andersen and Lindsley (1985, 1988) methods in the case of relatively reduced (ΔNNO < 1) magmas. The calculated temperature from the Ti-magnetite and ilmenite thermometry is compared with that calculated for the transitional type amphibole (Al_2O_3 = 9–11 wt%) and plagioclase (An = 40–45 mol%) pairs. For this, we used the edenite–richterite formulation (Holland and Blundy 1994; Anderson et al. 2008) because quartz is absent from the assemblage, and calculated temperatures between 790 and 830 °C (ESM 2). These calculated amphibole-plagioclase temperatures perfectly match those of the magnetite-ilmenite thermometry using the Andersen and Lindsley (1985) method for the Ee5/1–56 and Ee5/2–32 samples.

The amphibole zoning patterns clearly reflect a change in the magmatic conditions just before the eruption, which is likely to have caused re-equilibration of Ti-magnetite and ilmenite. In the studied pumice samples, both magnetite and ilmenite have resorbed margins and the surrounding glass is relatively enriched in Fe and Ti. This may record the pre-eruptive increase in temperature and/or change of the surrounding melt composition. Based on this observation, we suspect heating due to recharge by hot magma, which carried the magnesian amphibole (with inferred crystallization temperature > 900 °C) into the shallow, low-temperature (< 760 °C) magma reservoir. This magma recharge and mixing may then have ultimately initiated the eruptions. Temperatures of 790–830 °C calculated for magnetite-ilmenite pairs and amphibole-plagioclase rims of the hybrid magma are interpreted to reflect the temperature state immediately prior to and during the eruption.

Redox condition

The oxidation state of the magma reservoir is most commonly constrained by coexisting Ti-magnetite and ilmenite mineral pairs (Buddington and Lindsley 1964; Carmichael 1967; Powell and Powell 1977; Spencer and Lindsley 1981; Andersen and Lindsley 1985, 1988; Andersen et al. 1993; Ghiorso and Sack 1991; Ghiorso and Evans 2008). More recently, magmatic fO_2 is also commonly deduced using amphibole (Ridolfi et al. 2010; Goltz et al. 2022) and zircon (Loucks et al. 2018, 2020) as well as titanomagnetite-melt compositions (Arató and Audétat 2017a, b, c). Diffusion of main elements (e.g., Fe, Ti, Al, Mg, and Mn) occurs relatively rapidly in Fe-Ti oxides (on the timescale of hours to months; Venezky and Rutherford 1999; Morgado et al. 2019; Prissel et al. 2020; Hou et al. 2021), particularly in oxidized condition (Van Orman and Crispin 2010). Therefore, their chemical composition typically reflects the ultimate equilibrium condition prior to eruption. In contrast, other, slowly-equilibrating minerals (zircon, low-Al amphibole) can be used to constrain the long-term magma storage oxidation state.

In the Ciomadul dacitic pumices, Ti-magnetite and ilmenite have compositions consistent with equilibrium state based on the Bacon and Hirschmann (1988) test (Fig. S6). Although there are different calibrations (e.g., Andersen and Lindsley 1985, 1988; Ghiorso and Evans 2008) to calculate the oxygen fugacity, they gave similar results. The average calculated ΔNNO values range between + 1.0 and + 1.5 for the Ee5/1–56 and Ee5/2–32 units, whereas slightly higher values (+ 1.4 to + 1.8) are calculated for the Ee5/1–50 unit (Fig. S11). These results suggest relatively oxidized conditions for the Ciomadul magma reservoir just prior to eruption. Arató and Audétat (2017a, b, c) put forward two additional potential oxybarometers, which can be used in the absence of ilmenite. One of them (Arató and Audétat 2017a, b) is based on the partitioning of vanadium between magnetite and melt and can be applied within a wide temperature range for silicic magmas. The other one (FeTiMM; Arató and Audétat 2017c) uses Fe and Ti partitioning between magnetite and melt independent of temperature. Comparing the results of these oxybarometers with those obtained from the magnetite-ilmenite methods, a fairly good match can be observed with the FeTiMM results, although they are systematically shifted to lower fO_2 values by ca. 0.5 log units (ΔNNO values from the FeTiMM method are between + 0.6 and + 1.2 for the magnetite of the Ee5/1–56 and Ee5/2–32 units and from + 1.0 to + 1.6 in case of the Ee5/1–50 unit). On the contrary, the $V^{mgt-melt}$ oxybarometry gives significantly higher ΔNNO values (+ 1.8 – + 2.4 for the Ee5/1–56 and Ee5/2–32 eruption units). This might be due to the relatively high V content of the groundmass glass. Vanadium in magnetite has slower diffusion coefficient, and therefore does not re-equilibrate as the major elements (Sievwright et al. 2020). The glassy groundmass of the pumices has a V concentration of 10–16 ppm, possibly due to the magma recharge, whereas the V content of the highly evolved melt in the crystal mush reservoir beneath Ciomadul is fairly low, around 5 ppm, as determined for intercrystalline glass in felsic crystal clots of the older lava dome rocks. The $V^{mgt-melt}$ oxybarometry gives a perfect fit (ΔNNO = + 1.0 – + 1.5 for the Ee5/1–56 and Ee5/2–32 units) with that of the other techniques using the lower V content of the evolved glass (i.e., ~ 5 ppm), giving rise to a possible explanation that magnetite crystallized in the evolved crystal mush and re-equilibrated during magma recharge. Because of the slow diffusion of V, the $V^{mgt-melt}$ oxybarometry can be used to infer the pre-eruption low-temperature magma storage oxidation state with the V content of the evolved melt, whereas the other techniques based on the Fe–Ti distribution are more sensitive to the new equilibrium condition.

Following others, Loucks et al. (2018) suggested that the trace element composition of zircon also records the redox state of the magma reservoir. They proposed that zircon/melt partition coefficients of Ce and U change reversely in response to the variation of magma redox state and therefore, that the U/Pr and the Ce^{4+}/Ce^{3+} ratios provide information about fO_2 for low temperature mushy magma reservoirs. The Ciomadul zircon grains show high log U/Pr and log Ce^{4+}/Ce^{3+} values (3.9–4.9 and 2.2–3.7, respectively; calculated as proposed by Loucks et al. 2018; Fig. S12, ESM 2) suggesting oxidizing condition during zircon crystallization at low (680 to 790 °C) temperature. The calculated oxygen fugacity values (Loucks et al. 2020) are mostly between ΔNNO + 0.5 and + 1.5 at temperatures (680–740 °C) calculated using the Ferry and Watson (2007) Ti-in-zircon-thermometry. These oxygen fugacity values are slightly lower than those obtained from Fe-Ti-oxides and amphibole at slightly higher pre-eruptive temperature (Fig. 9). The oxidized state of the Ciomadul magma reservoir is reflected also by the trace element content of accessory minerals. Both zircon and titanite show only small negative Eu-anomaly (Eu/Eu* = 0.60–0.85 and 0.75–0.90, respectively) compared to those found in other silicic magma systems such as Kneeling Nun Tuff (Szymanowski et al. 2017) and Highland Range (Colombini et al. 2011) even though plagioclase crystallization was ubiquitous in the shallow magmatic system.

Amphibole composition is also sensitive to magmatic redox state (Humphreys et al. 2006). Ridolfi et al. (2010), Ridolfi and Renzulli (2012), and Ridolfi (2021) proposed empirical equations to calculate oxygen fugacity relative to the NNO buffer. These equations calculate, however, different values for our amphibole composition. Tests using experimental amphibole compositions suggest that the Ridolfi et al. (2010) method yields the most reasonable estimates to within ± 0.5 log units (Erdmann et al. 2014). Using

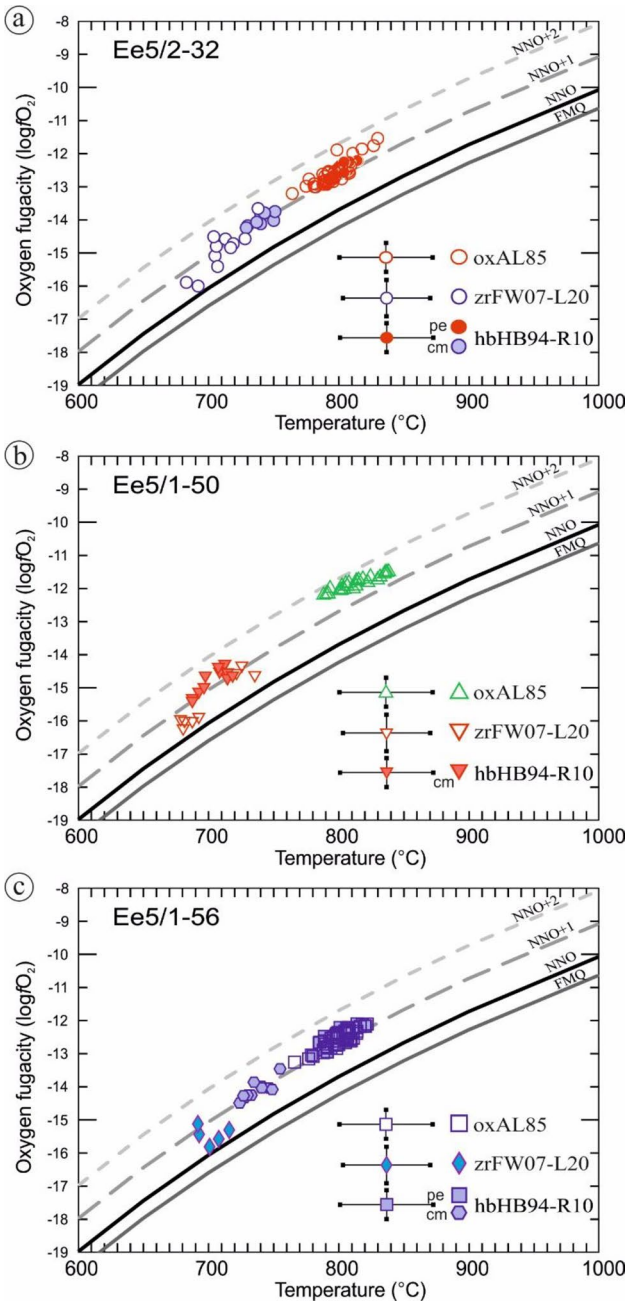

Fig. 9 Temperature (°C) vs. oxygen fugacity ($logfO_2$) plot for the three eruption units of Ciomadul **a**–**c** calculated by the following oxy- and thermobarometers: Andersen and Lindsley (1985) for Fe-Ti oxides (abbreviation: oxAL85); the combination of the Holland and Blundy (1994) thermometry and the Ridolfi et al. (2010) amphibole oxybarometry (abbreviation: hbHB94-R10), where amphiboles representing the crystal mush (cm) and pre-eruption (pe) conditions, respectively, are shown with different symbols; the combination of Ti-in-thermometry of Ferry and Watson (2007) and oxybarometry of Loucks et al. (2020) for zircon (abbreviation: zrFW07L20)

this oxybarometer, along with the temperature calculated from the Holland and Blundy (1994) thermometer the transitional amphibole group (mostly rim and microphenocryst core compositions that we interpret as pre-eruption amphibole) gives ΔNNO + 1.0 to + 1.5, which is consistent with the results of the Fe-Ti oxide oxythermobarometer (Fig. 9). Although we could not calculate oxidation state for the magnesian amphibole cores, which can represent the mafic recharge magma, their composition is similar to the high-Mg amphiboles of Shiveluch (crystallized at ~ ΔNNO + 2; Goltz et al. 2022), suggesting a high oxygen fugacity for the primitive melts.

In summary, we suggest that the oxygen fugacity and its variations in the Ciomadul magma plumbing system are robustly constrained by the different methods employed. We infer an oxidized state of ΔNNO + 1.0 to + 1.5 for the pre-eruptive magma, which concurs with estimates for other arc volcanic systems (Fish Canyon Tuff, Whitney and Stormer 1985; Johnson and Rutherford 1989b; Shiveluch, Humphreys et al. 2006; Mt St. Helens, Pallister et al. 2008; Longavi, Rodríguez et al. 2007; Mt Shasta, Grove et al. 2005). Zircon and amphibole oxybarometry results might indicate a slightly less oxidized state for the shallow crustal, felsic magma reservoir, but a more oxidized state of the magnesian amphibole-bearing recharge magmas. An increase in oxidation state is inferred from the magma mush to the reactivated pre-eruptive magma reservoir following magma mixing.

Melt compositions and H_2O contents

Calcic amphibole can occur in wide range of magmas and its composition is sensitive to melt composition and volatile content (e.g., Ridolfi et al. 2010; Ridolfi and Renzulli 2012; Putirka 2016; Zhang et al. 2017; Higgins et al. 2022). Ridolfi and Renzulli (2012) provided a set of equations to calculate equilibrium melt major element contents from amphibole compositional data. Based on tests using experimental amphibole and melt compositions, Erdmann et al. (2014) demonstrated the reliability of this calculation, particularly for melt SiO_2 content with an uncertainty of ± 4 wt% for SiO_2. Zhang et al. (2017) extended the experimental calibration data set and used multiple regression analyses to find the best fit between the compositional relationships of amphibole and melt composition. More recently, Higgins et al. (2022) applied nonlinear regression in a machine learning approach to determine melt composition in equilibrium with amphibole. This new calibration resulted in better constraints for melts with < 65 wt% SiO_2, where the Ridolfi and Renzulli (2012) equation yields slight overestimates. In the case of the Ciomadul pumice samples, a good fit between the calculated equilibrium melt and the glass data is found using the Higgins et al. (2022) method, particularly for SiO_2 and Al_2O_3 (Fig. 8c). However, the glass data for other elements show systematically slightly lower concentrations than the calculated compositions. The calculated melt compositions are in the range of 60 to 75 wt% SiO_2, showing an almost

continuous trend, whereas the measured glass compositions are only between 70 and 77 wt% SiO_2. This suggests that the inferred melt compositions provide additional insight into the magma evolution, which is not recorded by the glass data, neither the melt inclusion nor the matrix data set as pointed out also by Higgins et al. (2022) for the St. Kitts volcanics.

Our chemometry calculations confirm that the low-Al, low-Mg amphibole population crystallized from a highly evolved silicic melt (SiO_2 = 74–77 wt%) consistent with a low-temperature, near solidus crystal mush magmatic environment. The high-Mg amphibole group crystallized from less evolved melt (SiO_2 = 56–66 wt%) at higher temperature and greater depth as shown by the thermobarometric results. The transitional amphibole compositions of the phenocryst rims record final crystallization immediately prior to eruption from a moderately evolved silicic melt with an SiO_2 content of 68–70 wt%, which is the hybrid melt after rejuvenation and is represented by the groundmass glass of the Ee5/1–56 and Ee5/2–32 pumices, whereas the hybrid melt of the Ee5/1–50 pumice was more silicic (SiO_2 = 73–75 wt%; Fig. 8c).

The Ciomadul pumice samples have amphibole and biotite in addition to plagioclase macrocrysts. This implies that the melts contained a significant amount of H_2O, which can be estimated applying the plagioclase-melt hygrometer based on the latest calibration of Waters and Lange (2015). We used pressure values of 200–400 MPa and the average temperature calculated by amphibole-plagioclase thermometry (790–830 °C) in addition to plagioclase and inferred melt compositions as input parameters. The considered pressure variation does not significantly influence the calculated melt H_2O content (by < 0.3 wt% at 200–800 MPa range), whereas temperature has a significant control. A 30 °C change in the estimated temperature yields ± 1 wt% variation in the calculated melt H_2O content. Therefore, precise constraints on the thermal condition of the magma reservoir are very important and we can expect an uncertainty from the temperature determination. Plagioclase of the Ee5/1–50 unit are more sodic than those found in pumice from the other two eruption units, and they are associated with glasses showing a more evolved compositional character. Using an average calculated crystallization temperature of 730 °C, a fairly high melt H_2O content (6.9–7.1 wt%) is calculated. However, the result has to be considered with caution, since the inferred crystallization temperature is at the lower limit of the method (750 °C; Waters and Lange 2015), therefore, the uncertainty is much larger in this case. The plagioclase rim, which has fairly homogeneous composition (An = 40–50 mol%) in the Ee5/1–56 and the Ee5/2–32 units and the associated groundmass glass compositions could represent the pre-eruption magma condition. A temperature range of 790–830 °C was calculated from amphibole-plagioclase and magnetite-ilmenite thermometers. For an average temperature of 810 °C, the calculated melt H_2O content is between 5.4 and 5.9 wt%. Melt inclusions in amphibole and plagioclase show a wide range of volatile contents calculated by difference method (Devine et al. 1995; from 1 to 5 wt%), whereas for the groundmass glass has 4.0–6.5 wt% H_2O in the Ee5/1–50 pumice and from 0.5 to 6 wt% H_2O in the Ee5/1–56 and Ee5/2–32 pumice. This large range of estimated volatile (presumably mostly H_2O) content could record partial syn-eruptive degassing. Nevertheless, the upper values (5–6 wt%) are in agreement with the plagioclase-melt hygrometer results, suggesting a hydrous character of the pre-eruption Ciomadul magma. Rasmussen et al. (2022) demonstrated that magmatic water content controlled the pre-eruptive magma storage depth rather than neutral buoyancy. The presumed H_2O content of 5–6 wt% in the melt of the Ciomadul magma is slightly higher than found in most of the arc volcanoes compiled by Rasmussen et al. (2022). This infers a magma stalling depth between 8 and 12 km (based on Fig. 1 in Rasmussen et al. 2022), what fits well our calculated pressure values as well as the geophysical anomaly detected beneath Ciomadul (Popa et al. 2012; Harangi et al. 2015b).

The Ciomadul pumice contains high-Mg amphibole with high Mg# ($Mg^{2+}/(Mg^{2+} + Fe^{tot}) > 0.82$), which are rarely reported from volcanic eruption products worldwide. Grove et al. (2003) and Krawczynski et al. (2012) pointed out that such amphibole can crystallize from ultrahydrous magma (H_2O_{melt} = 10–15 wt%) as shown by their experiments using Mt Shasta magnesian andesite. More recently, Goltz et al. (2020) proposed that magmas erupted at Shiveluch were recharged by extremely H_2O-rich mafic magma (H_2O_{melt} = 10–14 wt%). In their studied mafic enclaves, amphibole with Mg# of up to 0.82 occur associated with olivine. H_2O-saturated experiments (Grove et al. 2003; Krawczynski et al. 2012) carried out between 200 and 800 MPa crystallize amphibole with a maximum Mg# of 0.82 as a near-liquidus phase. In the studied Ciomadul pumice, amphibole have Mg# often above 0.82, and this implies high dissolved melt H_2O content, comparable with that proposed for the Mt Shasta as well as the Shiveluch high-Mg andesitic to dacitic magmas.

Pre-eruptive magma conditions and recharge magma characteristics

Ciomadul is a typical long-dormant PAMS volcano, where a melt-bearing magma body is inferred to exist within the upper crust (Popa et al. 2012; Szakács and Seghedi 2013; Harangi et al. 2015b; Laumonier et al. 2019; Lukács et al. 2021). A careful evaluation of the textural and compositional characteristics of the mineral assemblages and application of various thermometers, barometers, oxybarometers, and

chemometers enable us to reconstruct the magma evolution and to constrain the intensive parameters at various stages of the magma condition.

During the youngest eruption episode (Eruptive epoch 5, i.e., Ee5; Molnár et al. 2019) of Ciomadul, a magma reservoir system is revealed with an upper crustal, felsic crystal mush body (at ~ 200–300 MPa, i.e., 8–12 km depth; Fig. 8d), underlain by accumulation storage zone of less evolved magmas at 400–1000 MPa (i.e., 16–40 km depth) as inferred also by Laumonier et al. (2019). The prolonged existence of felsic, near-solidus crystal mush body at the upper crust is inferred from zircon U-Th dates (Harangi et al. 2015a; Lukács et al. 2021) and from the presence of low-Al and low-Mg amphibole, sodic plagioclase, biotite, zircon and titanite in the erupted volcanic material. Such a long-lived, high-crystallinity hydrous magma body with similar mineral assemblage is common beneath andesitic to dacitic volcanoes (e.g., Fish Canyon Tuff, Bachmann et al. 2002; Mt St Helens, Thornber et al. 2008; Lamington, Humphreys et al. 2019; Savo, Smith 2014; Methana, Popa et al. 2020; Fig. 7). This magma reservoir beneath Ciomadul contains relatively cold (680–750 °C; constrained by zircon, titanite and amphibole-plagioclase thermometry) and slightly oxidized (+ 0.5 – + 1.5 ΔNNO, calculated from zircon and amphibole) crystal mush developed close to the wet solidus and this is consistent with the calculated present geothermic gradient (Rădulescu et al. 1981; Demetrescu and Andreescu 1994) and thermal modelling results (Laumonier et al. 2019). The interstitial melt was evolved, highly silicic, with an SiO_2 content of 70–77 wt% (as shown by the calculated equilibrium melt from low-Al amphibole and glass data; Fig. 8). In the amphibole population of the Ee5/1–56 and the Ee5/2–32 pumice, the high-Al, high-Mg and the transitional amphibole types dominate, which represent the recharge magma and the post-recharge overgrowth and microphenocrysts, respectively. Only minor amount of crystal mush-derived low-Al, low-Mg amphibole is present in the samples, and these crystals often show resorption, involving vermicular glass embayments (Fig. 4a, d, e, f, h). The plagioclase macrocrysts with spongy cellular texture (Fig. 2b, c) can also derive from the felsic crystal mush along with zircon and titanite. The strong resorption of these crystal mush-derived phases was due to the mixing followed by the recharge of a hot mafic to intermediate magma. Based on the relative amount of crystal types with different origin in the pumice samples, the low temperature crystal mush reservoir was mobilized to a lesser extent compared to the former 160–90 ka lava dome building stage. In contrast, the Ee5/1–50 pumices contain larger contributions from the felsic crystal mush. Their low-Al and low-Mg amphibole and An-poor plagioclase show large size, and they moreover occur in felsic crystal clots. Noteworthy, they do not show strong resorption and have comparable chemical compositions as those found in the older lava dome rocks (Fig. 7; Fig. S3; Kiss et al. 2014). In that case, the recharge magma was not as hot (> 900 °C) as in the other two explosive eruption events.

The high-Al and high-Mg amphibole population which represents the recharge magma in the studied Ee5/1–56 and Ee5/2–32 pumices is compositionally distinct (have lower Al^{IV} at the same Mg#) from the so-called pargasite group of the older lava dome rocks (Fig. 7; Kiss et al. 2014). Noteworthy, the magnesian amphiboles have Mg# > 0.82 (Figs. 7, 8a), which are even higher than those detected for amphibole of Mt Shasta (Grove et al. 2003, 2005), Shiveluch (Goltz et al. 2020; Gorbach et al. 2020) and Philippines and Baja California (Ribeiro et al. 2016) andesites. They are akin to the experimentally produced amphibole crystallized from ultrahydrous (H_2O > 10 wt%) magmas (Krawczynski et al. 2012). The Mg# of amphibole is controlled by the Fe/Mg ratio of the parental melt (Grove et al. 2003; Alonso-Perez et al. 2009) and Ribeiro et al. (2016, 2017) formulated an empirical equation for this relationship. Applying this equation, the high-Mg amphibole of Ciomadul may have crystallized from water-saturated primitive mantle melt, similarly to the amphiboles found in adakites (Hidalgo and Rooney 2010; Rooney et al. 2011; Ribeiro et al. 2016). Remarkably, this type of amphibole does not exist in the Ee5/1–50 pumice. Instead, a unique low-Al and high-Mg amphibole (Figs. 7, 8a) constitutes the core of the phenocrysts. Performing a thorough comparison with amphibole compositional data worldwide (GEOROC database, DIGIS Team 2022), no comparable amphibole composition in calc-alkaline volcanic rocks was found (Fig. 7). Instead, such amphibole occurs mostly in subarc metasomatized peridotites, such as in Avacha, Kamchatka (Ishimaru and Arai 2008; Ionov 2010; Benard et al. 2017; Siegrist et al. 2018) and Honshu arc, Japan (Endo et al. 2015). The only volcanic rocks that contain similar amphibole are adakites from Baja California (Ribeiro et al. 2016). Textural features of this type of amphibole (e.g., slight oscillatory zoning, continuous zoning boundary; Fig. 4f) in the Ciomadul pumice suggest their magmatic origin. The high Cr_2O_3 of this amphibole type can be explained by near-liquidus crystallization from a primary or near-primary hydrous melt from metasomatized, refractory peridotite.

The condition of the magmatic system just prior to eruption is constrained by the amphibole rim and microphenocryst population having a typical transitional composition (Fig. 5a), the relatively homogeneous plagioclase rim composition and the Ti-magnetite-ilmenite pairs because of their rapid equilibration. The crystal rims of amphibole in the studied pumices are 10–40 µm in width and considering various growth rate values (Zhang et al. 2019), they were formed within weeks to months before the explosive eruption. Noteworthy, the amphibole macrocryts do not have decompression-driven reaction rim, which is in turn

ubiquitous in the older lava dome rocks (Kiss et al. 2014). This, along with the relatively small amounts of microlites (≤ 13 vol%) suggests fast magma ascent. Line profiles across the Fe-Ti oxides indicate homogeneous composition (ESM 2), suggesting that they underwent a complete re-equilibration with the surrounding melt prior to eruption and it was preserved due to the rapid magma ascent. Fe-Ti oxide oxybarometry and thermometry imply that the magma was relatively oxidized at an average pre-eruptive temperature of 780–820 °C (Fig. 9). This estimate is confirmed by amphibole-plagioclase equilibrium pairs with the calculated average crystallization temperatures of 790–830 °C. Heating of the resident crystal mush by ~ 50–100 °C prior to eruption is explained by mixing with hot (> 900 °C) recharge magma, which transported magnesian amphibole crystal cargo, but no or minor plagioclase. Some portion of the felsic crystal mush incorporated into the recharge magma as shown by the reversely zoned amphibole crystals (Figs. 2e, 4a, h) and also by the positive correlation between An and FeO (Fig. 3) in the plagioclase composition (Ruprecht and Wörner 2007), particularly in the Ee5/1–56 and Ee5/2–32 units. However, these features cannot be seen in the Ee5/1–50 pumice, where plagioclase composition is restricted (20–35 mol% An; Fig. 3). We hypothesize that this can be due to the lower temperature of the recharge magma and the rapid reactivation process as shown by the very thin (< 20 µm) rim on the magnesian amphibole macrocrysts (Fig. 4f). In this case, only the Fe-Ti oxides indicate the heating effect along with an increase in the oxidation state.

Reasons of dominantly explosive eruptions

The eruption style strongly determines the associated volcanic hazard; therefore, it is crucial to understand better the controlling factors (Cassidy et al. 2018; Popa et al. 2021a, b). Whether a volcano erupts effusively or explosively strongly depends on conduit processes, i.e., whether gases can escape or remain trapped in the ascending magma (Gonnermann and Manga 2007; Wadsworth et al. 2020). Popa et al. (2021a, b) showed that crystallinity and the amount of dissolved H_2O in the melt have a major control, while Mangler et al. (2022) pointed out that the priming period, i.e., the timescale of recharge events prior to eruption may affect the style of eruption (e.g., in the case of Popocatépetl). The volcanic history of Ciomadul (YCEP stage; Molnár et al 2019) is subdivided into a lava dome building phase from 160 to 90 ka (Fig. 10a) and, following ca. 40 ka of quiescence, a dominantly explosive eruption phase from 56 to 30 ka (Fig. 10b). Textural and compositional features of the main mineral phases, particularly the amphibole imply that hot magma recharge triggered the eruptions, and a long-lived felsic crystal mush was variously involved in the reactivation processes.

The main differences between the effusive and explosive events of Ciomadul are the crystallinity of the erupted magma, the involvement of the felsic crystal mush and the nature of the recharge magma. In the case of the explosive eruptions, particularly in case of the Ee5/1–56 and the Ee5/2–32 phases, the erupted magma contained much lower proportions of crystals (< 40 vol% on vesicle-free basis), fewer antecrysts from the crystal mush (< 5 vol%) and the recharge magma was highly hydrous. Subtle differences can be recognized also within the pumices from the three studied eruption units, most notable is the extent of crystal mush involvement in the recharge magmas. After a 40 ka quiescence, the volcanic activity of Ciomadul reawakened by a massive explosive eruption series at 56 ka. At 50 ka, a presumably sub-Plinian explosive eruption resulted in thick pumice tephra, now exposed at Tuşnad. This event was triggered by a distinct recharge magma as shown by the strongly different amphibole composition (Fig. 5a) and involved more crystal mush material. The products of this eruption event were more silicic and only very narrow crystal rim growth are observed. This indicates that there was less time for hybridization and the eruption happened faster, than in the case of the 56 ka and 32 ka eruptions. Remarkably, during one of the latest explosive eruption phase at 32 ka, the pumices contained amphibole with strikingly similar compositional fingerprint as those in the 56 ka pumices, implying the return of a similar recharge magma as it was at 56 ka.

Each recharge magma was strongly hydrous from which near-liquidus, high-Mg amphibole crystallized. In general, such high-Mg amphibole occurs mostly in magnesian andesites and adakites (e.g., Mt. Shasta, Grove et al. 2003; Baja California, Ribeiro et al. 2016). Indeed, trace element composition of Ciomadul bulk rocks is consistent with adakitic features (Seghedi et al. 2004, 2023; Vinkler et al. 2007; Molnár et al. 2019). Noteworthy, these recharge magmas are different from those that initiated the older lava dome-forming effusive eruption events (Kiss et al. 2014). The strongly hydrous character of the magmas could lead to significant decrease of magma density and caused vesiculation (Grove et al. 2005), both contributing to the rapid ascent and to the explosive eruption style. The hydrous magmas interacted with the upper crustal felsic crystal mush to different degrees. In case of the 56 ka and 32 ka eruptions, the erupted magma was dominated by the recharge magma and only limited interaction occurred with the crystal mush, in a similar way as postulated by Popa et al. (2020) for the explosive events at Methana, Greece. These magma properties along with low crystallinity (< 40 vol% crystals on vesicle-free basis) favored rapid magma ascent and the explosive style eruption as predicted from the conditions determined by Popa et al. (2021a, b).

The unique magnesian amphibole compositions suggest that ultrahydrous primitive mantle-derived magmas could

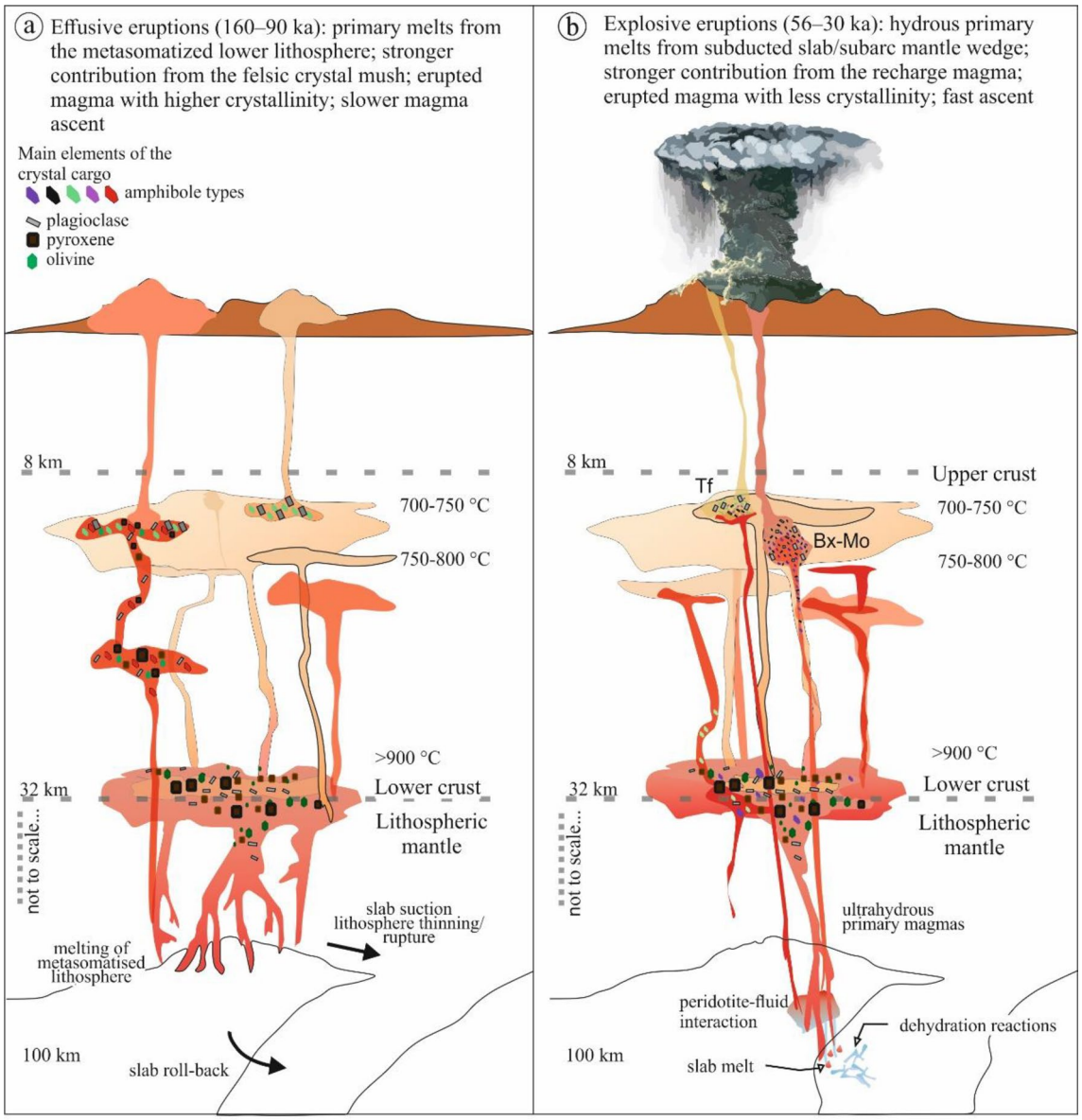

Fig. 10 Model for the magma reservoir architecture beneath Ciomadul constructed for the **a** dominantly effusive volcanic activities between 160 and 90 ka (following Kiss et al. 2014) and **b** dominantly explosive volcanic activity from 56 to 30 ka based on the physico-chemical constraints obtained by this study

play a major role in the 56–30 ka, mostly explosive volcanism of Ciomadul. In fact, such strongly hydrous magmas could have led to the transition from the mostly effusive to mostly explosive eruptions of the volcano. They contributed to keep the pre-eruption dissolved H_2O content of the melt at relatively high value (around 5.5 wt%) putting this condition at the upper limit of dominantly explosive eruptions (Popa et al. 2021a, b) at this eruptive epoch. Occurrence of strongly hydrous primitive magmas at this stage of the volcanism requires an increase of H_2O flux in the mantle during this period that remains to be further explored, although such specific condition is not unique as shown in case of the origin of the adakitic dacites at Nevado de Longaví volcano, Andes, Chile (Rodríguez et al. 2007). A possible explanation for the increased magmatic H_2O content/flux beneath Ciomadul could be the intensification of dehydration reactions in the Vrancea slab either reaching a depth of 100 km (Fig. 10), where various hydrous minerals break down during slab metamorphism and/or due to toroidal mantle flow around the narrow descending oceanic lithosphere body (Mason et al. 1998; Seghedi et al. 2011; Ferrand and Manea 2021). This could have induced even slab melting

and hydrous melt-peridotite reaction in the mantle wedge leading to primary magmas with adakitic compositional signature (Seghedi et al. 2023). Ferrand and Manea (2021) proposed that the deep earthquakes, which occur relatively frequently beneath the Vrancea zone could be induced by dehydration within an oceanic slab. If this model works, an important issue to be resolved is the timescales of dehydration intensification, sub-arc mantle melting, magma ascent and eruption triggering.

The outlined pre-eruption magma evolution model involving distinct recharge magma compared to the former 160–90 ka volcanism implies that each explosive eruption event was preceded by accumulation of mantle-derived magmas at the upper mantle-lower crustal region followed by ascent into the upper crustal reservoir. This would certainly cause seismic swarms from upper mantle to lower crustal hypocentres. Interaction within the upper crustal crystal mush reservoir, reheating and mixing of magmas can cause a change in the hypocentres, while volatile transfer and magma mixing result in overpressure and surface deformation. These sets of events are expected to commence only weeks to months prior to eruption, but they may remain undetected for non-monitored volcanic centers. Immediately prior to eruption, seismic events, degassing and surface deformation will increase significantly in magnitude and are likely detectable without specific instrumentation, but such warning may come too late. The sudden, unanticipated eruption of Chaitén in 2008 (Castro and Dingwell 2009) has provided a case example for non-monitored, long-dormant volcanoes, where warning signs at the surface appeared only hours before the explosive eruption.

Conclusions

(1) To reveal physicochemical conditions in subvolcanic magma reservoirs, a careful evaluation of applicable thermometers, barometers, oxybarometers, chemometers and hygrometers is necessary in addition to a comparison with relevant experimental data. While conditions for shallow, low temperature (< 800 °C), oxidized magma storage can be well constrained, conditions of the deep magma storage remain difficult to reconstruct.

(2) The crystal cargo of the studied Ciomadul dacitic pumices allows us to characterize the magma storage conditions for the pre-recharge, long-lived crystal mush body (low-Al amphibole, low-Ca plagioclase, zircon, titanite), the recharge magma (high-Mg amphibole) and also the post-recharge magma condition (Ti-magnetite, ilmenite, amphibole and plagioclase rims) just prior to eruption.

(3) The magma reservoir system beneath Ciomadul during the youngest, 56–30 ka eruption stage can be subdivided into an upper crustal felsic crystal mush body at 8–12 km depth with a slightly oxidized (0.5–1.6 ΔNNO), low-temperature (680–750 °C) highly crystalline magma and a deep magma storage with less evolved, hot (> 850 °C) magmas that partially crystallized at 16–40 km depth, at the crust–mantle boundary zone.

(4) The dominantly explosive volcanism following the entirely effusive eruptions in the previous volcanic epoch of Ciomadul can be explained by the ascent of distinct batches of highly hydrous recharge magmas. They contained high-Mg amphibole, which are inferred to have crystallized at near-liquidus conditions from ultrahydrous ($H_2O > 10$ wt%) magma. Such H_2O-rich primitive magma could have been generated due to the increase H_2O flux, probably as a result of intensification of dehydration reactions in the descending oceanic slab beneath the nearby Vrancea area. As a result, primary magmas with adakitic compositional features could have been generated by slab melting and/or hydrous melt-peridotite reaction in the mantle wedge.

(5) A detailed mineral-scale characterization of the complex magma storage system at various stages can help to better understand the behaviour of long-dormant volcanoes. In addition to the crystallinity and melt H_2O content of the pre-eruption magma, the nature of the recharge magma also plays an important role in the eruption style. These results can help in eruption forecasting and raise awareness of hazards of long-dormant volcanoes, where rapid rejuvenation can lead to volcanic eruption even after long quiescence.

Supplementary Information The online version contains supplementary material available at https://doi.org/10.1007/s00410-023-02075-z.

Acknowledgements This project has received funding from the HUN-REN Hungarian Research Network and financed directly by the Hungarian National Research Fund project (K 135179). BCs was supported by the ÚNKP-21-3 New National Excellence Program of the Ministry for Innovation and Technology. We are thankful to Andreas Kronz and Jochen Gätjen (Department of Geochemistry, University of Göttingen, Germany) for their assistance in the electron microprobe analyses, as well as to John Milan Hora (Czech Geological Survey) for helping in data processing and thermobarometric calculations of Fe-Ti oxides. Moreover, we are grateful to Róbert Arató (Institute for Nuclear Research, Debrecen, Hungary; University of Göttingen, Germany) for discussions and help regarding magnetite-melt oxybarometry. We gratefully acknowledge support by LabEx VOLTAIRE (LABX-100-01) and EquipEx PLANEX (ANR-11-EQPX-0036), which co-financed the mineral chemical analysis and the electron microprobe facility of ISTO-CNRS, Orléans. Personal consultations in Orléans were additionally sponsored by the Ministry of Foreign Affairs and Trade (Hungary) and the Embassy of Hungary in Paris with special thanks for Norbert Somogyi. Ioan Seghedi was supported by Romanian Executive Agency for Higher Education, Research, Development and Innovation Funding projects PN-III-P4-ID-PCCF-2016-0014. O. Bachmann acknowledges support of Swiss SNF grant #200020_214930 for this project. The

manuscript benefited from comments and suggestions provided by an anonymous reviewer and by Etienne Médard. We thank the editorial handling by prof. Timothy Grove.

Funding Open access funding provided by Eötvös Loránd University.

Data availability All data required will be made available.

Declarations

Conflict of interest The authors have no relevant financial or non-financial interests to disclose.

References

Alonso-Perez R, Müntener O, Ulmer P (2009) Igneous garnet and amphibole fractionation in the roots of island arcs: experimental constraints on andesitic liquids. Contrib Mineral Petrol 157:541–558. https://doi.org/10.1007/s00410-008-0351-8

Andersen DJ, Lindsley DH (1985) New (and final!) models for the Ti-magnetite/Ilmenite geothermometer and oxygen barometer. EOS Trans Am Geophys Union 66:416

Andersen DJ, Lindsley DH (1988) Internally consistent models for Fe-Mg-Mn-Ti oxides: Fe-Ti oxides. Amer Miner 73:714–726

Andersen DJ, Lindsley DH, Davidson PM (1993) QUILF: a pascal program to assess equilibria among Fe–Mg–Mn–Ti oxides, pyroxenes, olivine, and quartz. Comput Geosci 19:1333–1350. https://doi.org/10.1016/0098-3004(93)90033-2

Anderson JL, Smith DR (1995) The effects of temperature and fO2 on the Al-in-hornblende barometer. Amer Miner 80:549–559

Anderson JL, Barth AP, Wooden JL, Mazdab F (2008) Thermometers and thermobarometers in granitic systems. Rev Mineral Geochem 69:21–142. https://doi.org/10.2138/rmg.2008.69.4

Andrews BJ, Gardner JE (2010) Effects of caldera collapse on magma decompression rate: an example from the 1800 14C yr BP eruption of Ksudach Volcano, Kamchatka, Russia. J Volcanol Geotherm Res 198:205–216. https://doi.org/10.1016/j.jvolgeores.2010.08.021

Annen C, Blundy JD, Sparks RSJ (2006) The Genesis of Intermediate and Silicic Magmas in Deep Crustal Hot Zones. J Petrol 47:505–539. https://doi.org/10.1093/petrology/egi084

Arató R, Audétat A (2017a) Vanadium magnetite–melt oxybarometry of natural, silicic magmas: a comparison of various oxybarometers and thermometers. Contrib Mineral Petrol 172:1–22. https://doi.org/10.1007/s00410-017-1369-6

Arató R, Audétat A (2017b) Experimental calibration of a new oxybarometer for silicic magmas based on vanadium partitioning between magnetite and silicate melt. Geochim Cosmochim Acta 209:284–295. https://doi.org/10.1016/j.gca.2017.04.020

Arató R, Audétat A (2017c) FeTiMM—a new oxybarometer for mafic to felsic magma. Geochem Perspect Lett 5:19–23. https://doi.org/10.7185/geochemlet.1740

Bachmann O, Huber C (2016) Silicic magma reservoirs in the Earth's crust. Amer Miner 101:2377–2404. https://doi.org/10.2138/am-2016-5675

Bachmann O, Dungan MA, Lipman P (2002) The Fish Canyon Magma Body, San Juan Volcanic Field, Colorado: Rejuvenation and Eruption of an Upper-Crustal Batholith. J Petrol 43:1469–1503. https://doi.org/10.1093/petrology/43.8.1469

Bacon CR, Hirschmann MM (1988) Mg/Mn partitioning as a test for equilibrium between Fe-Ti oxides. Amer Miner 73:57–61

Benard A, Koga KT, Shimizu N, Kendrick MA, Ionov DA, Nebel O, Arculus RJ (2017) Chlorine and fluorine partition coefficients and abundances in sub-arc mantle xenoliths (Kamchatka, Russia): implications for melt generation and volatile recycling processes in subduction zones. Geochim Cosmochim Acta 199:324–350. https://doi.org/10.1016/j.gca.2016.10.035

Bindeman IN, Deegan FM, Troll VR, Thordarson T, Höskuldsson Á, Moreland WM, Zorn EU, Shevchenko AV, Walter TR (2022) Diverse mantle components with invariant oxygen isotopes in the 2021 Fagradalsfjall eruption, Iceland. Nat Commun 13:1–12. https://doi.org/10.1038/s41467-022-31348-7

Blundy JD, Holland TJ (1990) Calcic amphibole equilibria and a new amphibole-plagioclase geothermometer. Contrib Mineral Petrol 104:208–224. https://doi.org/10.1007/BF00306444

Blundy JD, Cashman KV, Berlo K (2008) Evolving Magma Storage Conditions Beneath Mount St. Helens Inferred from Chemical Variations in Melt Inclusions from the 1980–1986 and Current (2004–2006) Eruptions. A Volcano Rekindled: the Renewed Eruption of Mount St. Helens, 2004–2006. 33:755–790. https://doi.org/10.3133/pp175033

Buddington AF, Lindsley DH (1964) Iron-titanium oxide minerals and synthetic equivalents. J Petrol 5:310–357. https://doi.org/10.1093/petrology/5.2.310

Burgisser A, Bergantz GW (2011) A rapid mechanism to remobilize and homogenize highly crystalline magma bodies. Nature 471:212–215. https://doi.org/10.1038/nature09799

Cadoux A, Scaillet B, Druitt TH, Deloule E (2014) Magma storage conditions of large Plinian eruptions of Santorini Volcano (Greece). J Petrol 55:1129–1171. https://doi.org/10.1093/petrology/egu021

Carmichael ISE (1967) The iron-titanium oxides of salic volcanic rocks and their associated ferromagnesian silicates. Contrib Mineral Petrol 14:36–64. https://doi.org/10.1007/BF00370985

Cashman KV, Sparks RSJ (2013) How volcanoes work: a 25 year perspective. Bulletin 125:664–690. https://doi.org/10.1130/B30720.1

Cassidy M, Mani L (2022) Prepare now for big eruptions. Nature 608:469–471. https://doi.org/10.1038/d41586-022-02177-x

Cassidy M, Manga M, Cashman K, Bachmann O (2018) Controls on explosive-effusive volcanic eruption styles. Nat Commun 9:2839. https://doi.org/10.1038/s41467-018-05293-3

Castro JM, Dingwell DB (2009) Rapid ascent of rhyolitic magma at Chaitén volcano, Chile. Nature 461:780–783. https://doi.org/10.1038/nature08458

Chakraborty S, Dohmen R (2022) Diffusion chronometry of volcanic rocks: looking backward and forward. Bull Volcanol 84:1–9. https://doi.org/10.1007/s00445-022-01565-5

Colombini LL, Miller CF, Gualda GAR, Wooden JL, Miller JS (2011) Sphene and zircon in the Highland Range volcanic sequence (Miocene, southern Nevada, USA): elemental partitioning, phase relations, and influence on evolution of silicic magma. Mineral Petrol 102:29. https://doi.org/10.1007/s00710-011-0177-3

Conway CE, Chamberlain KJ, Harigane Y, Morgan DJ, Wilson CJN (2020) Rapid assembly of high-Mg andesites and dacites by

magma mixing at a continental arc stratovolcano. Geology 48:1033–1037. https://doi.org/10.1130/G47614.1

Coombs ML, Sisson TW, Bleick HA, Henton SM, Nye CJ, Payne AL, Cameron CE, Larsen JF, Wallace KL, Bull KF (2013) Andesites of the 2009 eruption of Redoubt Volcano, Alaska. J Volcanol Geotherm Res 259:349–372. https://doi.org/10.1016/j.jvolgeores.2012.01.002

Cooper KM (2019) Time scales and temperatures of crystal storage in magma reservoirs: implications for magma reservoir dynamics. Philos Trans R Soc London 377:20180009. https://doi.org/10.1098/rsta.2018.0009

Cooper KM, Kent AJR (2014) Rapid remobilization of magmatic crystals kept in cold storage. Nature 506:480–483. https://doi.org/10.1038/nature12991

Costa F, Scaillet B, Pichavant M (2004) Petrological and experimental constraints on the pre-eruption conditions of Holocene dacite from Volcán San Pedro (36 S, Chilean Andes) and the importance of sulphur in silicic subduction-related magmas. J Petrol 45:855–881. https://doi.org/10.1093/petrology/egg114

Costa F, Shea T, Ubide T (2020) Diffusion chronometry and the timescales of magmatic processes. Nat Rev Earth Environ 1:201–214. https://doi.org/10.1038/s43017-020-0038-x

Crisp LJ, Berry AJ (2022) A new model for zircon saturation in silicate melts. Contrib Mineral Petrol 177:1–24. https://doi.org/10.1007/s00410-022-01925-6

Demetrescu C, Andreescu M (1994) On the thermal regime of some tectonic units in a continental collision environment in Romania. Tectonophysics 230:26–276. https://doi.org/10.1016/0040-1951(94)90140-6

Devine JD, Gardner JE, Brack HP, Layne GD, Rutherford MJ (1995) Comparison of microanalytical methods for estimating H2O contents of silicic volcanic glasses. Am Mineral 80:319–328

Druitt TH, Costa F, Deloule E, Dungan M, Scaillet B (2012) Decadal to monthly timescales of magma transfer and reservoir growth at a caldera volcano. Nature 482:77–80. https://doi.org/10.1038/nature10706

Endo S, Mizukami T, Wallis SR, Tamura A, Arai S (2015) Orthopyroxene-rich Rocks from the Sanbagawa Belt (SW Japan): fluid-rock interaction in the forearc Slab-Mantle Wedge Interface. J Petrol 56:1113–1137. https://doi.org/10.1093/petrology/egv031

Erdmann S, Martel C, Pichavant M, Kushnir A (2014) Amphibole as an archivist of magmatic crystallization conditions: problems, potential, and implications for inferring magma storage prior to the paroxysmal 2010 eruption of Mount Merapi, Indonesia. Contrib Mineral Petrol 167:1016. https://doi.org/10.1007/s00410-014-1016-4

Erdmann S, Wang R, Huang F, Scaillet B, Zhao K, Liu H, Chen Y, Faure M (2019) Titanite: a potential solidus barometer for granitic magma systems. CR Geosci 351:551–561. https://doi.org/10.1016/j.crte.2019.09.002

Evans BW, Hildreth W, Bachmann O, Scaillet B (2016) In defense of magnetite-ilmenite thermometry in the Bishop Tuff and its implication for gradients in silicic magma reservoirs. Amer Miner 101:469–482. https://doi.org/10.2138/am-2016-5367

Ferrand TP, Manea EF (2021) Dehydration-induced earthquakes identified in a subducted oceanic slab beneath Vrancea, Romania. Sci Rep 11:1–9. https://doi.org/10.1038/s41598-021-89601-w

Ferry JM, Watson EB (2007) New thermodynamic models and revised calibrations for the Ti-in-zircon and Zr-in-rutile thermometers. Contrib Mineral Petrol 154:429–437. https://doi.org/10.1007/s00410-007-0201-0

Gansecki C, Lee RL, Shea T, Lundblad SP, Hon K, Parcheta C (2019) The tangled tale of Kīlauea's 2018 eruption as told by geochemical monitoring. Science 366:eaaz0147. https://doi.org/10.1126/science.aaz0147

Ghiorso MS, Evans BW (2008) Thermodynamics of rhombohedral oxide solid solutions and a revision of the Fe-Ti oxide geothermometer and oxygen-barometer. Am J Sci 308:957–1039. https://doi.org/10.2475/09.2008.01

Ghiorso MS, Sack RO (1991) Fe-Ti oxide geothermometry: thermodynamic formulation and the estimation of intensive variables in silicic magmas. Contrib Mineral Petrol 108:485–510. https://doi.org/10.1007/BF00303452

Giordano G, Caricchi L (2022) Determining the state of activity of transcrustal magmatic systems and their volcanoes. Annu Rev Earth Planet Sci. https://doi.org/10.1146/annurev-earth-032320-084733

Goltz AE, Krawczynski MJ, Gavrilenko M, Gorbach NV, Ruprecht P (2020) Evidence for superhydrous primitive arc magmas from mafic enclaves at Shiveluch volcano, Kamchatka. Contrib Mineral Petrol 175:1–26. https://doi.org/10.1007/s00410-020-01746-5

Goltz AE, Krawczynski MJ, McCanta MC, Dyar MD (2022) Experimental Calibration of an Fe^{3+}/Fe^{2+}-in-amphibole oxybarometer and its application to transcrustal magmatic processes at shiveluch volcano. Amer Miner in press, Kamchatka. https://doi.org/10.2138/am-2022-8031

Gonnermann HM, Manga M (2007) The fluid mechanics inside a volcano. Annu Rev Fluid Mech 39:321–356. https://doi.org/10.1146/annurev.fluid.39.050905.110207

Gorbach N, Philosofova T, Portnyagin M (2020) Amphibole record of the 1964 plinian and following dome-forming eruptions of Shiveluch volcano. Kamchatka J Volcanol Geotherm Res 407:107108. https://doi.org/10.1016/j.jvolgeores.2020.107108

Grove TL, Elkins-Tanton LT, Parman SW, Chatterjee N, Müntener O, Gaetani GA (2003) Fractional crystallization and mantle-melting controls on calc-alkaline differentiation trends. Contrib Mineral Petrol 145:515–533. https://doi.org/10.1007/s00410-003-0448-z

Grove TL, Baker MB, Price RC, Parman SW, Elkins-Tanton LT, Chatterjee N, Müntener O (2005) Magnesian andesite and dacite lavas from Mt. Shasta, northern California: products of fractional crystallization of H2O-rich mantle melts. Contrib Mineral Petrol 148:542–565. https://doi.org/10.1007/s00410-004-0619-6

Hammarstrom JM, Zen EA (1986) Aluminum in hornblende: an empirical igneous geobarometer. Am Miner 71:1297–1313

Harangi S (2001) Neogene to Quaternary volcanism of the Carpathian-Pannonian Region—a review. Acta Geol Hung 44:223–258

Harangi S, Lenkey L (2007) Genesis of the Neogene to Quaternary volcanism in the Carpathian-Pannonian region: role of subduction, extension, and mantle plume. In: Beccaluva L, Bianchini G, Wilson M (eds) Cenozoic volcanism in the mediterrean area. Geological Society of America. https://doi.org/10.1130/2007.2418(04)

Harangi S, Molnár M, Vinkler AP, Kiss B, Jull AJT, Leonard AG (2010) Radiocarbon dating of the last volcanic eruptions of Ciomadul volcano, Southeast Carpathians, eastern-central Europe. Radiocarbon 52:1498–1507. https://doi.org/10.1017/S0033822200046580

Harangi S, Lukács R, Schmitt AK, Dunkl I, Molnár K, Kiss B, Seghedi I, Novothny Á, Molnár M (2015a) Constraints on the timing of Quaternary volcanism and duration of magma residence at Ciomadul volcano, east-central Europe, from combined U-Th/He and U/Th zircon geochronology. J Volcanol Geotherm Res 301:66–80. https://doi.org/10.1016/j.jvolgeores.2015.05.002

Harangi S, Novák A, Kiss B, Seghedi I, Lukács R, Szarka L, Wesztergom V, Metwaly M, Gribovszki K (2015b) Combined magnetotelluric and petrologic constrains for the nature of the magma storage system beneath the Late Pleistocene Ciomadul volcano (SE Carpathians). J Volcanol Geotherm Res 290:82–96. https://doi.org/10.1016/j.jvolgeores.2014.12.006

Harangi S, Molnár K, Schmitt AK, Dunkl I, Seghedi I, Novothny Á, Molnár M, Kiss B, Ntaflos T, Mason PRD, Lukács R (2020) Fingerprinting the Late Pleistocene tephras of Ciomadul volcano, eastern–central Europe. J Quat Sci 35:232–244. https://doi.org/10.1002/jqs.3177

Hawthorne FC, Oberti R, Harlow GE, Maresch WV, Martin RF, Schumacher JC, Welch MD (2012) Nomenclature of the amphibole supergroup. Am Min 97:2031–2048. https://doi.org/10.2138/am.2012.4276

Hayden LA, Watson EB, Wark DA (2008) A thermobarometer for sphane (titanite). Contrib Mineral Petrol 155:529–540. https://doi.org/10.1007/s00410-007-0256-y

Hidalgo PJ, Rooney TO (2010) Crystal fractionation processes at Baru volcano from the deep to shallow crust. Geochem Geophys Geosyst. https://doi.org/10.1029/2010GC003262

Higgins O, Sheldrake T, Caricchi L (2022) Machine learning thermobarometry and chemometry using amphibole and clinopyroxene: a window into the roots of an arc volcano (Mount Liamuiga, Saint Kitts). Contrib Mineral Petrol 177:1–22. https://doi.org/10.1007/s00410-021-01874-6

Holland TJB, Blundy JD (1994) Non-ideal interactions in calcic amphiboles and their bearing on amphibole-plagioclase thermometry. Contrib Mineral Petrol 116:433–447. https://doi.org/10.1007/BF00310910

Hollister LS, Grissom GC, Peters EK, Stowell HH, Sisson VB (1987) Confirmation of the empirical correlation of Al in hornblende with pressure of solidification of calc-alkaline plutons. Am Miner 72:231–239

Hou T, Botcharnikov R, Moulas E, Just T, Berndt J, Koepke J, Zhang Z, Wang M, Yang Z, Holtz F (2021) Kinetics of Fe–Ti oxide re-equilibration in magmatic systems: implications for thermo-oxybarometry. J Petrol 61:1–24. https://doi.org/10.1093/petrology/egaa116

Humphreys MC, Blundy JD, Sparks RSJ (2006) Magma evolution and open-system processes at Shiveluch Volcano: Insights from phenocryst zoning. J Petrol 47:2303–2334. https://doi.org/10.1093/petrology/egl045

Humphreys MCS, Cooper GF, Zhang J, Loewen M, Kent AJR, Macpherson CG, Davidson JP (2019) Unravelling the complexity of magma plumbing at Mount St. Helens: a new trace element partitioning scheme for amphibole. Contrib Mineral Petrol. https://doi.org/10.1007/s00410-018-1543-5

Ionov DA (2010) Petrology of mantle wedge lithosphere: new data on supra-subduction zone peridotite xenoliths from the andesitic Avacha volcano, Kamchatka. J Petrol 51:327–361. https://doi.org/10.1093/petrology/egp090

Ishimaru S, Arai S (2008) Calcic amphiboles in peridotite xenoliths from Avacha volcano, Kamchatka, and their implications for metasomatic conditions in the mantle wedge. Geol Soc Lon Specl Publ 293:35–55. https://doi.org/10.1144/SP293.3

Johnson MC, Rutherford MJ (1989a) Experimental calibration of the aluminium-in-hornblende geobarometer with application to Long Valley caldera (California) volcanic rocks. Geology 17:837–841. https://doi.org/10.1130/0091-7613(1989)017%3c0837:ECOTAI%3e2.3.CO;2

Johnson MC, Rutherford MJ (1989b) Experimentally determined conditions in the fish canyon tuff, colorado, magma chamber. J Petrol 30:711–737. https://doi.org/10.1093/petrology/30.3.711

Karátson D, Wulf S, Veres D, Magyari EK, Gertisser R, Timar-Gabor A, Novothny Á, Telbisz T, Szalai Z, Anechitei-Deacu V, Appelt O, Bormann M, Cs J, Hubay K, Schäbitz F (2016) The latest explosive eruptions of Ciomadul (Csomád) volcano, East Carpathians—a tephrostratigraphic approach for the 51–29 ka BP time interval. J Volcanol Geotherm Res 319:29–51. https://doi.org/10.1016/j.jvolgeores.2016.03.005

Karátson D, Telbisz T, Dibacto S, Lahitte P, Szakács A, Veres D, Gertisser R, Cs J, Timár G (2019) Eruptive history of the Late Quaternary Ciomadul (Csomád) volcano, East Carpathians, part II: magma output rates. Bull Volcanol 81:28. https://doi.org/10.1007/s00445-019-1287-8

Kis BM, Ionescu A, Cardellini C, Harangi S, Baciu C, Caracausi A, Viveiros F (2017) Quantification of carbon dioxide emissions of Ciomadul, the youngest volcano of the Carpathian-Pannonian Region (Eastern-Central Europe, Romania). J Volcanol Geoth Res 341:119–130. https://doi.org/10.1016/j.jvolgeores.2017.05.025

Kis BM, Caracausi A, Palcsu L, Baciu C, Ionescu A, Futó I, Sciarra A, Harangi S (2019) Noble gas and carbon isotope systematics at the seemingly inactive Ciomadul volcano (Eastern-Central Europe, Romania): evidence for volcanic degassing. Geochem Geophys 20:3019–3043. https://doi.org/10.1029/2018GC008153

Kiss B, Harangi S, Ntaflos T, Mason PRD, Pál-Molnár E (2014) Amphibole perspective to unravel pre-eruptive processes and conditions in volcanic plumbing systems beneath intermediate arc volcanoes: a case study from Ciomadul volcano (SE Carpathians). Contrib Mineral Petrol 167:986. https://doi.org/10.1007/s00410-014-0986-6

Klaver M, Matveev S, Berndt J, Lissenberg CJ, Vroon PZ (2017) A mineral and cumulate perspective to magma differentiation at Nisyros volcano, Aegean arc. Contrib Mineral Petrol 172:1–23. https://doi.org/10.1007/s00410-017-1414-5

Konečný V, Kováč M, Lexa J, Šefara J (2002) Neogene evolution of the Carpatho-Pannonian region: an interplay of subduction and back-arc diapiric uprise in the mantle. EGU Stephan Mueller Spec Publ Ser 1:105–123

Krawczynski MJ, Grove TL, Behrens H (2012) Amphibole stability in primitive arc magmas: effects of temperature, H2O content, and oxygen fugacity. Contrib Mineral Petrol 164:317–339. https://doi.org/10.1007/s00410-012-0740-x

Lahitte P, Dibacto S, Karátson D, Gertisser R, Veres D (2019) Eruptive history of the Late Quaternary Ciomadul (Csomád) volcano, East Carpathians, part I: timing of lava dome activity constrained by the unspiked K-Ar method. Bull Volcanol 81:1–28. https://doi.org/10.1007/s00445-019-1286-9

Laumonier M, Karakas O, Bachmann O, Gaillard F, Lukács R, Seghedi I, Menand T, Harangi S (2019) Evidence for a persistent magma reservoir with large melt content beneath an apparently extinct volcano. Earth Planet Sci Lett 521:79–90. https://doi.org/10.1016/j.epsl.2019.06.004

Leake BE, Woolley AR, Arps CES, Birch WD, Gilbert MC, Grice JD, Hawthorne FC, Kato A, Kisch HJ, Krivovichev VG, Linthout K, Laird J, Mandarino J, Maresch WV, Nickel EH, Rock NMS, Schumacher JC, Smith DC, Stephenson NCN, Ungaretti L, Whittaker EJW, Youzhi G (1997) Nomenclature of amphiboles; report of the subcommittee on amphiboles of the international mineralogical association commission on new minerals and mineral names. Mineral Mag 61:295–310. https://doi.org/10.1180/minmag.1997.061.405.13

Locock AJ (2014) An Excel spreadsheet to classify chemical analyses of amphiboles following the IMA 2012 recommendations. Comput Geosci 62:1–11. https://doi.org/10.1016/j.cageo.2013.09.011

Loucks RR, Fiorentini ML, Rohrlach BD (2018) Divergent T–$fO2$ paths during crystallisation of H2O-rich and H2O-poor magmas as recorded by Ce and U in zircon, with implications for TitaniQ and TitaniZ geothermometry. Contrib Mineral Petrol 173:104. https://doi.org/10.1007/s00410-018-1529-3

Loucks RR, Fiorentini ML, Henríquez GJ (2020) New magmatic oxybarometer using trace elements in zircon. J Petrol. https://doi.org/10.1093/petrology/egaa034

Lukács R, Caricchi L, Schmitt AK, Bachmann O, Karakas O, Guillong M, Molnár K, Seghedi I, Harangi S (2021) Zircon geochronology suggests a long-living and active magmatic system beneath the Ciomadul volcanic dome field (eastern-central Europe). Earth Planet Sci Lett 565:116965. https://doi.org/10.1016/j.epsl.2021.116965

Mangler MF, Petrone CM, Prytulak J (2022) Magma recharge patterns control eruption styles and magnitudes at Popocatépetl volcano (Mexico). Geology 50:366–370. https://doi.org/10.1130/G49365.1

Mani L, Tzachor A, Cole P (2021) Global catastrophic risk from lower magnitude volcanic eruptions. Nat Commun 12:1–5. https://doi.org/10.1038/s41467-021-25021-8

Mason PRD, Downes H, Seghedi I, Szakács A, Thirlwall MF (1995) Low-pressure evolution of magmas from the Calimani, Gurghiu and Harghita Mountains, East Carpathians. Acta Vulcanol 7:43–52

Mason PRD, Downes H, Thirlwall MF, Seghedi I, Szakács A, Lowry D, Mattey D (1996) Crustal assimilation as a major petrogenetic process in east Carpathian Neogene to Quaternary continental margin arc magmas. J Petrol 37:927–959. https://doi.org/10.1093/petrology/37.4.927

Mason PRD, Seghedi I, Szakács A, Downes H (1998) Magmatic constraints on geodynamic models of subduction in the East Carpathians, Romania. Tectonophysics 297:157–176. https://doi.org/10.1016/s0040-1951(98)00167-x

Maţenco L, Bertotti G (2000) Tertiary tectonic evolution of the external East Carpathians (Romania). Tectonophysics 316:255–286. https://doi.org/10.1016/S0040-1951(99)00261-9

Matthews NE, Huber C, Pyle DM, Smith VC (2012) Timescales of magma recharge and reactivation of large silicic systems from Ti diffusion in Quartz. J Petrol 53:1385–1416. https://doi.org/10.1093/petrology/egs020

Médard E, Le Pennec JL (2022) Petrologic imaging of the magma reservoirs that feed large silicic eruptions. Lithos 428:106812. https://doi.org/10.1016/j.lithos.2022.106812

Melekhova E, Blundy J, Robertson R, Humphreys MC (2015) Experimental evidence for polybaric differentiation of primitive arc basalt beneath St. Vincent, Lesser Antilles. J Petrol 56:161–192. https://doi.org/10.1093/petrology/egu074

Molina JF, Moreno JA, Castro A, Rodríguez C, Fershtater GB (2015) Calcic amphibole thermobarometry in metamorphic and igneous rocks: new calibrations based on plagioclase/amphibole Al-Si partitioning and amphibole/liquid Mg partitioning. Lithos 232:286–305. https://doi.org/10.1016/j.lithos.2015.06.027

Molnár K, Harangi S, Lukács R, Dunkl I, Schmitt AK, Kiss B, Garamhegyi T, Seghedi I (2018) The onset of the volcanism in the Ciomadul Volcanic Dome Complex (Eastern Carpathians): eruption chronology and magma type variation. J Volcanol Geotherm Res 354:39–56. https://doi.org/10.1016/j.jvolgeores.2018.01.025

Molnár K, Lukács R, Dunkl I, Schmitt AK, Kiss B, Seghedi I, Szepesi J, Harangi S (2019) Episodes of dormancy and eruption of the Late Pleistocene Ciomadul volcanic complex (Eastern Carpathians, Romania) constrained by zircon geochronology. J Volcanol Geotherm Res 373:133–147. https://doi.org/10.1016/j.jvolgeores.2019.01.025

Morgado E, Morgan DJ, Castruccio A, Ebmeier SK, Parada M-Á, Brahm R, Harvey J, Gutiérrez F, Walshaw R (2019) Old magma and a new, intrusive trigger: using diffusion chronometry to understand the rapid-onset Calbuco eruption, April 2015 (Southern Chile). Contrib Mineral Petrol 174:61. https://doi.org/10.1007/s00410-019-1596-0

Morgan DJ, Blake S, Rogers NW, De Vivo B, Rolandi G, Davidson JP (2006) Magma chamber recharge at Vesuvius in the century prior to the eruption of A.D. 79. Geology 34:845–848. https://doi.org/10.1130/G22604.1

Murphy MD, Sparks RSJ, Barclay J, Carroll MR, Brewer TS (2000) Remobilization of andesite magma by intrusion of mafic magma at the Soufriere Hills Volcano, Montserrat, West Indies. J Petrol 41:21–42. https://doi.org/10.1093/petrology/41.1.21

Mutch EJF, Blundy JD, Tattitch BC, Cooper FJ, Brooker RA (2016) An experimental study of amphibole stability in low-pressure granitic magmas and a revised Al-in-hornblende geobarometer. Contrib Mineral Petrol 171:1–27. https://doi.org/10.1007/s00410-016-1298-9

Nagasaki S, Ishibashi H, Suwa Y, Yasuda A, Hokanishi N, Ohkura T, Takemura K (2017) Magma reservoir conditions beneath Tsurumi volcano, SW Japan: evidence from amphibole thermobarometry and seismicity. Lithos 278:153–165. https://doi.org/10.1016/j.lithos.2017.01.011

Newhall C, Self S, Robock A (2018) Anticipating future Volcanic Explosivity Index (VEI) 7 eruptions and their chilling impacts. Geosphere 14:572–603. https://doi.org/10.1130/GES01513.1

Nurfiani D, Wang X, Gunawan H, Triastuty H, Hidayat D, Wei SJ, Taisne B, de Bouvet Maisonneuve C (2021) Combining petrology and seismology to unravel the plumbing system of a typical arc volcano: an example from Marapi West Sumatra Indonesia. Geochem Geophys Geosy 22:e2020GC009524. https://doi.org/10.1029/2020GC009524

Pallister JS, Hoblitt RP, Meeker GP, Knight RJ, Siems DF (1996) Magma mixing at mount pinatubo: petrographic and chemical evidence from the 1991 deposits, fire and mud. Eruptions and Lahars of Mount Pinatubo Philippines. University of Washington Press, pp 687–732

Pallister JS, Thornber CR, Cashman KV, Clynne MA, Lowers H, Mandeville CW, Brownfield IK, Meeker GP (2008) Petrology of the 2004–2006 Mount St. Helens lava dome–Implications for magmatic plumbing and eruption triggering 1750–30, 647–702. US Geological Survey. https://doi.org/10.3133/pp175030

Pankhurst MJ, Scarrow JH, Barbee OA, Hickey J, Coldwell BC, Rollinson GK, Rodríguez-Losada JA, Martín Lorenzo A, Rodríguez F, Hernández W, Calvo Fernández D, Hernández PA, Pérez NM (2022) Rapid response petrology for the opening eruptive phase of the 2021 Cumbre Vieja eruption, La Palma, Canary Islands. Volcanica 5:1–10. https://doi.org/10.30909/vol.05.01.0110

Papale P, Marzocchi W (2019) Volcanic threats to global society. Science 363:1275–1276. https://doi.org/10.1126/science.aaw7201

Paton C, Hellstrom J, Paul B, Woodhead J, Hergt J (2011) Iolite: freeware for the visualisation and processing of mass spectrometric data. J Anal at Spectrom 26:2508–2518. https://doi.org/10.1039/C1JA10172B

Pécskay Z, Lexa J, Szakács A, Seghedi I, Balogh K, Konečný V, Zelenka T, Kovács M, Póka T, Fülöp A, Márton E, Panaiotu C, Cvetković V (2006) Geochronology of Neogene magmatism in the Carpathian arc and intra-Carpathian area. Geol Carpath 57:511

Pichavant M, Macdonald R (2007) Crystallization of primitive basaltic magmas at crustal pressures and genesis of the calc-alkaline igneous suite: experimental evidence from St Vincent, Lesser Antilles arc. Contrib Mineral Petrol 154:535–558. https://doi.org/10.1007/s00410-007-0208-6

Pichavant M, Martel C, Bourdier JL, Scaillet B (2002) Physical conditions, structure, and dynamics of a zoned magma chamber: Mount Pelée (Martinique Lesser Antilles Arc). J Geophys Res Solid Eart. https://doi.org/10.1029/2001JB000315

Poland MP, Anderson KR (2020) Partly cloudy with a chance of lava flows: forecasting volcanic eruptions in the twenty-first century. J Geophys Res Solid Earth. https://doi.org/10.1029/2018JB016974

Popa M, Radulian M, Szakács A, Seghedi I, Zaharia B (2012) New seismic and tomography data in the southern part of the Harghita Mountains (Romania, Southeastern Carpathians): connection

with recent volcanic activity. Pure Appl Geophys 169:1557–1573. https://doi.org/10.1007/s00024-011-0428-6

Popa R-G, Bachmann O, Ellis BS, Degruyter W, Tollan P, Kyriakopoulos K (2019) A connection between magma chamber processes and eruptive styles revealed at Nisyros-Yali volcano (Greece). J Volcanol Geotherm Res 387:106666. https://doi.org/10.1016/j.jvolgeores.2019.106666

Popa R-G, Dietrich VJ, Bachmann O (2020) Effusive-explosive transitions of water-undersaturated magmas. The case study of Methana Volcano, South Aegean Arc. J Volcanol Geotherm Res 399:106884. https://doi.org/10.1016/j.jvolgeores.2020.106884

Popa R-G, Bachmann O, Huber C (2021a) Explosive or effusive style of volcanic eruption determined by magma storage conditions. Nature Geosci 14:781–786. https://doi.org/10.1038/s41561-021-00827-9

Popa RG, Tollan P, Bachmann O, Schenker V, Ellis B, Allaz JM (2021b) Water exsolution in the magma chamber favors effusive eruptions: application of Cl-F partitioning behavior at the Nisyros-Yali volcanic area. Chem Geol 570:120170. https://doi.org/10.1016/j.chemgeo.2021.120170

Powell R, Powell M (1977) Geothermometry and oxygen barometry using coexisting iron-titanium oxides: a reappraisal. Mineral Mag 41:257–263. https://doi.org/10.1180/minmag.1977.041.318.14

Prissel KB, Krawczynski MJ, Van Orman JA (2020) Fe–Mg and Fe–Mn interdiffusion in ilmenite with implications for geospeedometry using oxides. Contrib Mineral Petrol 175:62. https://doi.org/10.1007/s00410-020-01695-z

Prouteau G, Scaillet B (2003) Experimental constraints on the origin of the 1991 Pinatubo dacite. J Petrol 44:2203–2241

Putirka KD (2008) Thermometers and barometers for volcanic systems. Rev Mineral Geochem 69:61–120. https://doi.org/10.2138/rmg.2008.69.3

Putirka K (2016) Amphibole thermometers and barometers for igneous systems and some implications for eruption mechanisms of felsic magmas at arc volcanoes. Am Miner 101:841–858. https://doi.org/10.2138/am-2016-5506

Rădulescu D, Péter E, Stanciu C, Ştefănescu M, Veliciu Ş (1981) Asupra anomaliilor geotermice din sudul muntilor Harghita. Studii Cercetari Geol Geofizice 26:169–184

Rasmussen DJ, Plank TA, Roman DC, Zimmer MM (2022) Magmatic water content controls the pre-eruptive depth of arc magmas. Science 375:1169–1172. https://doi.org/10.1126/science.abm5174

Ribeiro JM, Maury RC, Grégoire M (2016) Are adakites slab melts or high-pressure fractionated mantle melts? J Petrol 57:839–862. https://doi.org/10.1093/petrology/egw023

Ribeiro JM, Maury RC, Grégoire M (2017) Corrigendum to: are adakites slab melts or high-pressure fractionated mantle melts? J Petrol 58:189–190. https://doi.org/10.1093/petrology/egx010

Ridolfi F (2021) Amp-TB2: an updated model for calcic amphibole thermobarometry. Minerals 11:324. https://doi.org/10.3390/min11030324

Ridolfi F, Renzulli A (2012) Calcic amphiboles in calc-alkaline and alkaline magmas: thermobarometric and chemometric empirical equations valid up to 1,130 °C and 2.2 GPa. Contrib Mineral Petrol 163:877–895. https://doi.org/10.1007/s00410-011-0704-6

Ridolfi F, Renzulli A, Puerini M (2010) Stability and chemical equilibrium of amphibole in calc-alkaline magmas: an overview, new thermobarometric formulations and application to subduction-related volcanoes. Contrib Mineral Petrol 160:45–66. https://doi.org/10.1007/s00410-009-0465-7

Rodríguez C, Sellés D, Dungan M, Langmuir C, Leeman W (2007) Adakitic dacites formed by intracrustal crystal fractionation of water-rich parent magmas at Nevado de Longaví volcano (36.2°S; Andean Southern Volcanic Zone, Central Chile). J Petrol 48:2033–2061. https://doi.org/10.1093/petrology/egm049

Roduit N (Accessed 2022) JMicroVision: image analysis toolbox for measuring and quantifying components of high-definition images. Version 1.3.4. https://jmicrovision.github.io

Rooney TO, Franceschi P, Hall CM (2011) Water-saturated magmas in the Panama Canal region: a precursor to adakite-like magma generation? Contrib Mineral Petrol 161:373–388. https://doi.org/10.1007/s00410-010-0537-8

Roure F, Roca E, Sassi W (1993) The Neogene evolution of the outer Carpathian flysch units (Poland, Ukraine and Romania): kinematics of a foreland/fold-and-thrust belt system. Sediment Geol 86:177–201. https://doi.org/10.1016/0037-0738(93)90139-V

Royden LH, Horvath F, Burchfiel BC (1982) Transform faulting, extension, and subduction in the Carpathian Pannonian region. Geol Soc Am Bull 93:717–725. https://doi.org/10.1130/0016-7606(1982)93%3c717:TFEASI%3e2.0.CO;2

Ruprecht P, Wörner G (2007) Variable regimes in magma systems documented in plagioclase zoning patterns: El Misti stratovolcano and Andahua monogenetic cones. J Volcanol Geotherm Res 165:142–162. https://doi.org/10.1016/j.jvolgeores.2007.06.002

Rutherford MJ, Devine JD (1996) Pre-eruption pressure-temperature conditions and volatiles in the 1991 Dacitic Magma of Mount Pinatubo. In: Newhall C, Punongbayan R (eds) Fire and mud: eruptions and Lahars of Mount Pinatubo, Philippines: Seattle. University of Washington Press, pp 751–766. https://doi.org/10.1016/j.jvolgeores.2007.06.002

Sato H, Holtz F, Behrens H, Botcharnikov R, Nakada S (2005) Experimental petrology of the 1991–1995 Unzen dacite, Japan. Part II: Cl/OH partitioning between hornblende and melt and its implications for the origin of oscillatory zoning of hornblende phenocrysts. J Petrol 46:339–354. https://doi.org/10.1093/petrology/egh078

Saunders K, Blundy J, Dohmen R, Cashman K (2012) Linking petrology and seismology at an active volcano. Science 336:1023–1027. https://doi.org/10.1126/science.1220066

Scaillet B, Evans BW (1999) The 15 June 1991 eruption of Mount Pinatubo. I. Phase equilibria and pre-eruption P-T–f O2–f H2O conditions of the dacite magma. J Petrol 40:381–411. https://doi.org/10.1093/petroj/40.3.381

Schmidt MW (1992) Amphibole composition in tonalite as a function of pressure: an experimental calibration of the Al-in-hornblende barometer. Contrib Mineral Petrol 110:304–310. https://doi.org/10.1007/BF00310745

Schumacher JC (1997) Appendix 2: the estimation of ferric iron in the electron-microprobe analysis of amphiboles. Can Mineral 35:238–246

Seghedi I, Downes H (2011) Geochemistry and tectonic development of Cenozoic magmatism in the Carpathian-Pannonian region. Gondwana Res 20:655–672. https://doi.org/10.1016/j.gr.2011.06.009

Seghedi I, Szakács A, Udrescu C, Stoian M, Grabari G (1987) Trace element geochemistry of the South Hargitha volcanics (East Carpathians): calc-alkaline and shoshonitic association. Dari Seama Ale Sedintelor Inst Geol Geofizica 72–73:381–397

Seghedi I, Balintoni I, Szakacs A (1998) Interplay of tectonics and neogene post-collisional magmatism in the intracarpathian region. Lithos 45:483–497. https://doi.org/10.1016/S0024-4937(98)00046-2

Seghedi I, Downes H, Szakács A, Mason PRD, Thirlwall MF, Roşu E, Pécskay Z, Marton E, Panaiotu C (2004) Neogene-Quaternary magmatism and geodynamics in the Carpathian-Pannonian region: a synthesis. Lithos 72:117–146. https://doi.org/10.1016/j.lithos.2003.08.006

Seghedi I, Maţenco L, Downes H, Mason PR, Szakács A, Pécskay Z (2011) Tectonic significance of changes in post-subduction Pliocene-Quaternary magmatism in the south east part of the

Carpathian-Pannonian Region. Tectonophysics 502:146–157. https://doi.org/10.1016/j.tecto.2009.12.003
Seghedi I, Besutiu L, Mirea V, Zlagnean L, Popa R-G, Szakács A, Atanasiu L, Pomeran M, Vişan M (2019) Tectono-magmatic characteristics of post-collisional magmatism: case study East Carpathians, Călimani-Gurghiu-Harghita volcanic range. Phys Earth Planet Inter 293:106270. https://doi.org/10.1016/j.pepi.2019.106270
Seghedi I, Lukács R, Soós I, Guilong M, Bachmann O, Cserép B, Harangi S (2023) Magma evolution in a complex geodynamic setting, South Harghita volcanic area, East-Central Europe: constraints from magma compositions and zircon petrochronology. Lithos 442–443:107059. https://doi.org/10.1016/j.lithos.2023.107059
Siegrist MT, Yogodzinski G, Bizimis M, Churikova T (2018) Ce-anomalies, elevated Ba/Th, Metasomatic Orthopyroxenite, and variably Depleted Indian-Type MORB Mantle in Mafic and Ultramafic Xenoliths from Kharchinsky Volcano, Kamchatka. In AGU Fall Meeting Abstracts T21G-0300
Sievwright RH, O'Neill HSC, Tolley J, Wilkinson JJ, Berry AJ (2020) Diffusion and partition coefficients of minor and trace elements in magnetite as a function of oxygen fugacity at 1150 ºC. Contrib Min Petrol 175:40. https://doi.org/10.1007/s00410-020-01679-z
Smith DJ (2014) Clinopyroxene precursors to amphibole sponge in arc crust. Nat Commun 5:1–6. https://doi.org/10.1038/ncomms5329
Sparks RSJ (2003) Forecasting volcanic eruptions. Earth Planet Sci Lett 210:1–15. https://doi.org/10.1016/S0012-821X(03)00124-9
Spencer KJ, Lindsley DH (1981) A solution model for coexisting iron–titanium oxides. Am Miner 66:1189–1201. https://doi.org/10.1038/ncomms5329
Sundermeyer C, Di Muro A, Gordeychik B, Wörner G (2019) Time-scales of magmatic processes during the eruptive cycle 2014–2015 at Piton de la Fournaise, La Réunion, obtained from Mg–Fe diffusion modelling in olivine. Contrib Mineral Petrol 175:1. https://doi.org/10.1007/s00410-019-1642-y
Szabó C, Harangi S, Csontos L (1992) Review of neogene and quaternary volcanism of the Carpathian-Pannonian region. Tectonophysics 208:243–256. https://doi.org/10.1016/0040-1951(92)90347-9
Szakács A, Seghedi I (1989) Base surge deposits in the Ciomadul Massif (South Harghita Mts.). DS Inst Geol Geofiz 74:175–180
Szakács A, Seghedi I (2013) The relevance of volcanic hazard in Romania: is there any? Environ Eng Manag J 12:125–135. https://doi.org/10.30638/eemj.2013.015
Szakács A, Seghedi I, Pécskay Z (1993) Peculiarities of South Harghita Mts. as the terminal segment of the Carpathian Neogene to Quaternary volcanic chain. Rev Roum Géol Géophys Géograph Géol 37:21–37
Szakács A, Seghedi I, Pécskay Z (2002) The most recent volcanism in the Carpatho-Pannonian region. Is there any volcanic hazard? Geol Carp 53:193–194
Szakács A, Seghedi I, Pécskay Z, Mirea V (2015) Eruptive history of low-frequency and low-output rate Pleistocene volcano, Ciomadul, South Harghita Mts. Romania Bull Volcanol 77:1–19. https://doi.org/10.1007/s00445-014-0894-7
Szymanowski D, Wotzlaw J-F, Ellis BS, Bachmann O, Guillong M, von Quadt A (2017) Protracted near-solidus storage and pre-eruptive rejuvenation of large magma reservoirs. Nature Geosci 10:777–782. https://doi.org/10.1016/J.Chemgeo.2018.02.001
Thornber CR, Pallister JS, Lowers HA, Rowe MC, Mandeville CW, Meeker GP, Sherrod DR (2008) Chemistry, mineralogy, and petrology of amphibole in Mount St. Helens 2004–2006 dacite. A volcano rekindled, 2004–2006. https://doi.org/10.3133/pp175032
Tiepolo M, Tribuzio R, Langone A (2011) High-Mg andesite petrogenesis by amphibole crystallization and ultramafic crust assimilation: evidence from adamello hornblendites (Central Alps, Italy). J Petrol 52:1011–1045. https://doi.org/10.1093/petrology/egr016
Van Orman JA, Crispin KL (2010) Diffusion in oxides. Rev Min Geochem 72:757–825. https://doi.org/10.2138/rmg.2010.72.17
Venezky DY, Rutherford MJ (1999) Petrology and Fe-Ti oxide reequilibration of the 1991 Mount Unzen mixed magma. J Volcanol Geotherm Res 89:213–230. https://doi.org/10.1016/S0377-0273(98)00133-4
Vinkler AP, Harangi S, Ntaflos T, Szakács A (2007) A Csomád vulkán (Keleti-Kárpátok) horzsaköveinek kőzettani és geokémiai vizsgálata—petrogenetikai következtetések. Földtani Közlöny 137:103–128
Wadsworth FB, Llewellin EW, Vasseur J, Gardner JE, Tuffen H (2020) Explosive-effusive volcanic eruption transitions caused by sintering. Sci Adv 6:eaba7940. https://doi.org/10.1126/sciadv.aba7940
Waters LE, Lange RA (2015) An updated calibration of the plagioclase-liquid hygrometer-thermometer applicable to basalts through rhyolites. Am Miner 100:2172–2184. https://doi.org/10.2138/am-2015-5232
Watson EB, Harrison M (1983) Zircon saturation revisited: temperature and composition effects in a variety of crustal magma types. Earth Planet Sci Lett 64:295–304
Wenzel F, Achauer U, Enescu D, Kissling E, Russo R, Mocanu V, Musacchio G (1998) Detailed look at final stage of plate breakoff is target of study in Romania. Eos Trans Am Geophys Union 79:589–594
Whitney A, Stormer JC Jr (1985) Mineralogy, petrology, and magmatic conditions from the fish Canyon Tuff, central San Juan volcanic field, Colorado. J Petrol 26:726–752. https://doi.org/10.1093/petrology/26.3.726
Wieser P, Petrelli M, Lubbers J, Wieser E, Ozaydin S, Kent A, Till C (2022) Thermobar: an open-source Python3 tool for thermobarometry and hygrometry. Volcanica 5:349–384. https://doi.org/10.30909/vol.05.02.349384
Wieser PE, Kent AJ, Till C, Donovan J, Neave DA, Blatter D, Krawczynski MM (2022) Barometers behaving badly: assessing the influence of analytical and experimental uncertainty on clinopyroxene thermobarometry calculations at crustal conditions. J Petrol. https://doi.org/10.31223/X5JT0N
Zellmer GF (2021) Gaining acuity on crystal terminology in volcanic rocks. Bull of Volcanol 83:78. https://doi.org/10.1007/s00445-021-01505-9
Zhang J, Humphreys MCS, Cooper GF, Davidson JP, Macpherson CG (2017) Magma mush chemistry at subduction zones, revealed by new melt major element inversion from calcic amphiboles. Am Miner 102:1353–1367. https://doi.org/10.2138/am-2017-5928
Zhang B, Hu X, Asimow PD, Zhang X, Xu J, Fan D, Zhou W (2019) Crystal size distribution of amphibole grown from hydrous basaltic melt at 0.6–2.6 GPa and 860–970°C. Am Miner 104:525–535. https://doi.org/10.1007/s11631-019-00322-4

Authors and Affiliations

Barbara Cserép[1,2] · Máté Szemerédi[1,3] · Szabolcs Harangi[1,2] · Saskia Erdmann[4] · Olivier Bachmann[5] · István Dunkl[6] · Ioan Seghedi[7] · Katalin Mészáros[2] · Zoltán Kovács[1,8] · Attila Virág[2,9] · Theodoros Ntaflos[10] · David Schiller[11] · Kata Molnár[12] · Réka Lukács[1,13]

✉ Szabolcs Harangi
harangi.szabolcs@ttk.elte.hu

Barbara Cserép
cserep.barbara@gmail.com

Máté Szemerédi
szemeredi.mate@gmail.com

Saskia Erdmann
saskia.erdmann@cnrs-orleans.fr

Olivier Bachmann
olivier.bachmann@erdw.ethz.ch

István Dunkl
istvan.dunkl@geo.uni-goettingen.de

Ioan Seghedi
seghedi@geodin.ro

Katalin Mészáros
kata.meszaros92@gmail.com

Zoltán Kovács
kozraat@gmail.com

Attila Virág
viragattila.pal@gmail.com

Theodoros Ntaflos
theodoros.ntaflos@univie.ac.at

David Schiller
david.schiller@stud.sbg.ac.at

Kata Molnár
molnar.kata@atomki.hu

Réka Lukács
lukacs.reka@csfk.org

[1] HUN-REN-ELTE Volcanology Research Group, Pázmány Péter sétány 1/C, 1117 Budapest, Hungary

[2] Department of Petrology and Geochemistry, Institute of Geography and Earth Sciences, Eötvös Loránd University, Pázmány Péter sétány 1/C, 1117 Budapest, Hungary

[3] Department of Mineralogy, Geochemistry and Petrology, 'Vulcano' Petrology and Geochemistry Research Group, University of Szeged, Egyetem utca 2, 6722 Szeged, Hungary

[4] Institut des Sciences de la Terre d'Orléans (ISTO), Université d'Orléans-CNRS-BRGM, UMR 7327, Orléans, France

[5] Department of Earth Sciences, Institute of Geochemistry and Petrology, ETH Zürich, Zurich, Switzerland

[6] Department of Sedimentology and Environmental Geology, Geoscience Center, University of Göttingen, Goldschmidtstr. 3, 37077 Göttingen, Germany

[7] Institute of Geodynamics Sabba S. Ştefanescu, Romanian Academy, 19-23 Jean-Luis Calderon St., Bucharest-37, Romania

[8] HUN-REN Centre for Energy Research, Konkoly-Thege Miklós út 29-33, 1121 Budapest, Hungary

[9] Department of Mineralogy and Geology, Institute of Earth Sciences, University of Debrecen, Egyetem tér 1, 4032 Debrecen, Hungary

[10] Department of Lithospheric Research, University of Vienna, Althanstrasse 14, 1090 Vienna, Austria

[11] Department of Chemistry and Physics of Materials, University of Salzburg, Jakob-Haringer-Strasse 2a, 5020 Salzburg, Austria

[12] Isotope Climatology and Environmental Research Centre, HUN-REN Institute for Nuclear Research, Bem tér 18/C, Debrecen 4026, Hungary

[13] Institute for Geological and Geochemical Research, HUN-REN Research Centre for Astronomy and Earth Sciences (MTA Centre of Excellence), Budaörsi út 45, 1112 Budapest, Hungary